UNIVERSIDADE FEDERAL DE SANTA CATARINA
PROGRAMA DE PÓS GRADUAÇÃO EM CIÊNCIA E ENGENHARIA DE MATERIAIS

Mylena Mayara Matias Carrijo

MANUFACTURING Ti_3SiC_2-BASED COMPOSITES VIA THREE-DIMENSIONAL PRINTING: PROCESSING AND CHARACTERIZATION

Thesis submitted to the Graduate Program in Materials Science and Engineering at Federal University of Santa Catarina for obtaining the Master's Degree in Materials Science and Engineering.

Adivisor: Prof. Dr. Guilherme Mariz de Oliveira Barra

Co-Adivisor: Prof. Dr. Dachamir Hotza

Co-Adivisor: Dr: Nahum Travitzky

Florianopolis

2015

I dedicate this work to my family.

ACKNOWLEDGEMENT

Primarily I would like to thank God who afforded me the chance to do what I most love. To my parents, Edmilson Matias and Claudia Matias, and my brother, Pedro Felipe Matias, for always supporting me unreservedly.

I would like to express my gratitude to my supervisor in Brazil Prof. Dr. Guilherme Mariz de Oliveira Barra, who was always fully ready to help independent of the situation or location. For the friendship through these 3 years that we have been working together, the opportunity to make part of his research group, for orientation and for all the knowledge shared. Thank you very much.

To my supervisor in Germany Dr. Nahum Travitzky, who promptly received me in his Rapid Prototyping research group in WW3 at Friedrich-Alexander-Universität Erlangen-Nürnberg to develop the experimental procedure of this work. Thank you very much for providing me a wonderful experience, for all the support in my academic and personal life, for the patience and for all the given teachings.

I would like to thank Ina Filbert-Demut, who helped me every day with my experiments and research. Thanks for the possibility to work with you, for the friendship, support, patience and all the given knowledge.

I would like to say thanks to Prof. Dr. Dachamir Hotza who provided me the opportunity to develop this work in Germany and for all the support.

I also would like to thank my boyfriend, Hannes Lorenz. For the companionship during the write process, all help and patience.

I would like to say thank to my colleagues from Composites and Polymers Laboratory: Adriana Silveira, Bruna Rosa, Claudia Merlini, Daliana Muller, Giseli Contri, Patricia Vargas, Scheyla Kuester, Silvia Ramôa and Rodrigo Cercená. My colleagues from WW3: Dr. Tobias Fey, Karin Bichler, Alexander Bonet, Benjamin Dermeik, Franziska Eichhorn, Ruth Hammerbacher, Daniel Jakobsen, Lorenz Schlier, Alfons Stiegelschmitt, Bodo Zierath, Sabine Brungs, Andreas Thomsen, Thimotheus Nunes, Heiko Huber, Hunter Rauch, Lukas Weiß, Julia Groppweis, Theresa Eder, Florens Bach, Marita Lenhart, Corinna Böhm, Jan Schultheiß and Eva Springer. For the great work environment, relaxation moments and help.

Finally I would like to thank the Federal University of Santa Catarina, the Graduate Program in Materials Science and Engineering, Friedrich-Alexander-Universität Erlangen-Nürnberg and the National

Council for Scientific and Technological Development (CAPES) for the infrastructure and financial support.

Nothing in life is to be feared, it is only to be understood.

(Marie Curie)

RESUMO

Compósitos de Ti_3SiC_2 foram fabricados por meio de três passos principais de processamento: (i) impressão tridimensional de mistura em pó de Ti_3SiC_2-dextrina, (ii) prensagem isostática a frio e uniaxial e (iii) sinterização. A mistura Ti_3SiC_2-dextrina foi primeiramente impressa através de impressão (jato de tinta indireta) tridimensional. As amostras impressas foram submetidas a dois processos de prensagem diferentes: isostática a frio e prensagem uniaxial. Por um lado, três conjuntos de amostras impressas foram submetidas a prensagem isostática a frio (CIP) a 180 MPa, a 150 MPa e 35 MPa. Por outro lado, um outro conjunto de amostras impressa foram submetida a prensagem uniaxial a 726 MPa. No último passo do processamento, amostras prensadas uniaxialmente e isotaticamente a frio e um conjunto de amostra impressas comparativa - sem processo de prensagem - foram expostas a sinterização a 1600 ° C em atmosfera de argônio durante 2 horas. Análise de difracção de raios X (XRD) mostrou Ti_3SiC_2 como fase principal em todas as amostras depois dos três estágios de processamento, mas também apresentou $TiC_{0,63}$ como fase secundária. Composição química da fase por espectroscopia de raios-X de energia dispersiva (EDS) também indicaram presença de SiC como fase secundária em todas as amostras, o que foi verificado por microscopia eletrônica de varredura (MEV). Assim, o que indica que o Ti3SiC2 na presença de carbono - descendente a partir de dextrina - decompõe-se em TiC0.63, SiC e Si (g). Além disso SEM mostrou a distribuição de fases das amostras em cada etapa de processamento e apresentou maior densidade e presença de rachaduras em espécimes uniaxialmente pressadas. As medidas de porosidade, densidade, variação de massa e retração após cada etapa de processamento, mostraram que os compósitos de Ti_3SiC_2 uniaxialmente pressionados obteve a maior densidade, igual 98,2% em massa. O módulo de elasticidade e resistência à flexão também são maiores para compósitos uniaxialmente.

Palavras-chave: Ti_3SiC_2, impressão tridimensional, prensagem isostática a frio, prensagem uniaxial, sinterização.

ABSTRACT

Ti_3SiC_2-based composites were fabricated via three main steps processing: (i) three-dimensional printing of Ti_3SiC_2-dextrin powder mixture, (ii) cold isostatic and uniaxial pressing and (iii) sintering. Ti_3SiC_2-dextrin powder blend was first printed via three-dimensional (indirect ink-jet) printing. The printed specimens were submitted to two different pressing processes, such as cold isostatic and uniaxial pressing. On the one hand three printed sets were submitted to cold isostatic pressing (CIP) at 180 MPa, 150 MPa and 35 MPa. On the other hand another printed sample set was submitted to uniaxial pressing at 726 MPa. In the last step of the processing, uniaxially and cold isostatic pressed samples and one comparative printed sample set - without pressing process - were exposed to sintering at 1600 °C in argon atmosphere for 2 hours. X-ray diffraction (XRD) analysis showed Ti_3SiC_2 as main phase in all specimens after three stages processing, but also presented $TiC_{0,63}$ as a secondary phase. Phase's chemical composition by energy-dispersive X-ray spectroscopy (EDS) indicated also presence of SiC as secondary phase in all samples, which was verified by scanning electron microscopy (SEM). Thus, indicating that the Ti_3SiC_2 in presence of carbon – descendant from dextrin – decomposes in $TiC_{0.63,}$ SiC and $Si_{(g)}$. Besides that SEM showed the phase distribution of specimens in each steps of processing and presented higher density and presence of cracks in uniaxially pressed specimens. The measurements of porosity, density, weight loss and shrinkage after each steps showed that uniaxially pressed Ti_3SiC_2-based structures obtained the highest density, equal 98.2 wt%. Young's modulus and flexural strength are also higher for uniaxially pressed Ti_3SiC_2-based composites.

Keywords: Ti_3SiC_2, three-dimensional printing, cold isostatic pressing, uniaxial pressing, sintering.

LIST OF FIGURES

LIST OF TABLES

LIST OF ABBREVIATIONS

2D	two-dimensional
3D	three-dimensional
3DP	three-dimensional printing
BTP	brittle-to-plastic transition
CAD	computer-aided design
CAM	computer-aided manufacturing
CIP	cold isostatic pressing
CVD	chemical vapor deposition
DTA	differential thermal analysis
EDX	energy-dispersive X-ray spectroscopy
FDM	fused deposition modelling
HIP	hot isostatic pressing
HP	hot pressing
LOM	laminated object manufacturing
PVC	polyvinyl chloride
SEM	scanning electron microscopy
SLS	selective laser sintering
STL	standard tessellation language
TGA	thermogravimetric analysis
XRD	X-ray diffraction

SUMÁRIO

1. INTRODUTION

Titanium silicon carbide, Ti_3SiC_2, is characteristic of a ternary ceramic belonging to the class of layered ternary carbides and/or nitrides known as MAX Phase (RADOVIC and BARSOUM, 2013; EL-RAGHY and BARSOUM, 1998). This material has been noticed by the combination of mechanical, electrical and thermal properties of both metals and ceramics. Thereby they provide excellent thermal shock resistance, high electrical and thermal conductivity, oxidation resistant, thermal and chemical resistance, high stiffness, easily machinable, great refractory, low hardness and high Young's Modulus (EL-RAGHY and BARSOUM, 1996; LIS *et al.*, 1997; EL-RAGHY and BARSOUM, 1998; GAO, LI *et al*., 2002). It is also machinable as graphite, at room temperature it shows brittle failure behavior and at 1300 °C plastic behavior (EL-RAGHY and BARSOUM, 1999).

Jeitschko and Nowotny were the firsts to synthesize Ti_3SiC_2 via chemical reaction between TiH_2, Si, and graphite at 2000°C (JEITSCHKO and NOWOTNY, 1967). Nowadays studies have shown that Ti_3SiC_2 can be obtained by chemical vapor deposition (CVD), combustion synthesis, reactive sintering, hot isostatic pressing (HIP), hot pressing and spark plasma sintering from the raw powders (TONG *et al*., 1995; EL-RAGHY and BARSOUM, 1996; LIS et al., 1997; GAO et al., 2002; SUN, DCOSTA and EL-RAGHY, 2002). Beyond the synthesis methods above, the final product is usually Ti_3SiC_2 in powder form. Thus, for the manufacturing of three-dimensional structures the powder consolidation techniques are required.

For forming ceramic powder with the aim to obtain three-dimensional structures the conventional powder consolidation techniques present a few limitations, for example: manufacturing of complex-shaped ceramics parts, difficulties to achieve highly dense structure and the use of hard tooling die and casting mold, which for its own fabrication can have high cost and time-consuming processes (SUN, DCOSTA and EL-RAGHY, 2002). In this context, three-dimensional printing (3DP) emerged as a cheaper and faster alternative to produce ceramics bodies with complex geometry without high energy, lasers and/or any toxic materials. The process can also be adapted to a variety of powders in order to create the desired pore size, and shape (TAY, EVANS and EDIRISINGHE, 2003; MELCHER *et al*., 2011). 3DP consists in the addition of the desired material by point until the required object is finished without the need of mold or die walls. A CAD modelling

computed tomography scanning is required to produce the two-dimensional (2D) profile and then the objects can be created via layered printing. The process is based on the principle of ink-jet printing, which has two methods: direct and indirect ink-jet printing. In direct ink-jet printing, a suspension of ceramic powder and a volatile liquid is used as an ink and it is printed on a substrate capable to absorb this suspension. In indirect ink-jet printing, the ink is a binder solution, which is printed onto the powder layer; binding the powder particles to one another and consequently, the cross-section one level below. In both methods this process is repeated until the body is finished (TAY, EVANS and EDIRISINGHE, 2003; MELCHER *et al*., 2011).

However, in 3DP the density of final product can be influenced by the particle size, layer thickness and saturation of binder (MELCHER *et al.*, 2006). There are alternatives to increase the density, for examples: sintering of green samples, modifying the binder or powders and including intermediate pressing process before sintering.

The sintering process is commonly used to increase density of green materials, which consists in the pores elimination due the atomic diffusion given by capillary forces in adjacent particles (CHEN and WANG, 2000). Besides of the pores decrease, sintering can also offer the possible to synthesize ceramic compounds from their elemental powder (GAO *et al*., 2002) and also provide the microstructure development of bodies from ceramic compounds prior synthesized leading to the formation of new final phases and consequently different properties.

Another alternative to improve the final densification of samples after 3DP it is the pressing process as, uniaxial and cold isostatic pressing. Isostatic pressing technique has been a viable and cheap path to consolidate powder composites. Within the isostatic pressing technique, the cold isostatic pressing is commonly used as intermediary step and consists in the immersion of capsuled samples in a pressure tank filled with an aqueous suspension (TURNER and ASHBY, 1996). Thereby the samples are subject a hydraulically isostatic pressure providing a significant densification. The isostatic pressing advantages consist in capability to process immiscible systems, capability to process composites covering high-melting point materials and diffusive alterations can be avoid by choosing the proper pressure-temperature-time cycle. Furthermore, it is possible to produce a fine-grained material with a uniform microstructure; complex geometries can be made to near-net shape and for arbitrarily powder mixture, an isotropic composite can be reached (TURNER and ASHBY, 1996). In uniaxial pressing the desired powder can be placed between two rigid punch faces and die walls

for the compaction. The steps of uniaxial pressing consist in (i) die filling, (ii) compaction and (iii) ejection of the compact. It is possible to carry out via hydraulic or mechanical compaction press and the advantages include mass production of accuracy parts and low cost technique (RIEDEL and CHEN, 2012).

Based on the above, this work utilizes post-processing treatments after 3DP in order to improve density of Ti_3SiC_2-based composites. Isostatic and uniaxial pressing processes were chosen as an intermediary stage and sintering as a final stage processing. Besides that, the influence on densification and microstructural properties of final specimens were investigated.

1.1. OBJECTIVES

1.1.1. General objectives

Study and investigation of the manufacturing process of Ti_3SiC_2-based composites process via three-dimensional printing, cold isostatic and uniaxial pressing, and sintering.

1.1.2. Specific objectives

- Manufacturing of Ti_3SiC_2-dextrin solid freeform composites via three-dimensional printing with indirect ink-jet technology;
- Evaluating of the effect of cold isostatic and uniaxial pressing as an intermediary process on the final product densities;
- Correlating the influence of two different pressing process on the final parts properties.

2. FUNDAMENTALS

2.1. TITANIUM SILICON CARBIDE

Titanium Silicon Carbide, Ti_3SiC_2, is a ternary ceramic belonging to MAX Phase class. MAX Phases are known as layered ternary carbides and nitrides which have chemical formula equal $M_{n+1}AX_n$, where n= 1, 2 or 3; M is transition metal; A is element from the non-metal group of the Periodic Table Elements (subset of elements 13-16) and X is either carbon and/or nitrogen (EL-RAGHY and BARSOUM 1998; SUN, 2011; RADOVIC and BARSOUM, 2013). Ti_3SiC_2 is so far the most studied MAX Phase, which is characteristic of a layered hexagonal crystal structures with two TiC octaehdral layers separated by planar Si layer (Fig 1) (EL-RAGHY *et al*., 1997; RILEY *et al*. 2002).

Figure 1- Ti3SiC2 unit cell.

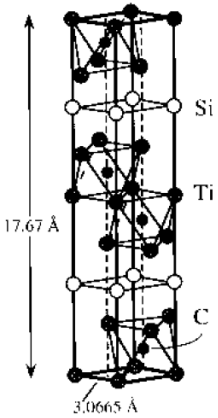

Source: (EL-RAGHY *et al.* 1997)

Due to the combination of metallic, covalent and ionic bonds, this material is a good example of a metal-ceramic system (ARANUJATESAN and CARIM, 1995; RADOVIC and BARSOUM, 2013; ABU, MOHAMED and AHMAD, 2014). It has also been noticed by the combination of mechanical, electrical and thermal properties of both metals and ceramics. Thereby it provides high electrical and thermal conductivity. It is easily machinable without cooling or lubrication; low hardness; thermal shock resistance; damage tolerance and ductility

typical of ductile metals. High Young's Modulus, high temperature strength and oxidation and corrosion resistant is characteristic of ceramics (EL-RAGHY and BARSOUM, 1996; LIS *et al*. 1997; EL-RAGHY and BARSOUM, 1998; EL-RAGHY and BARSOUM, 1999; ZHOU and SUN, 2000; GAO *et al*., 2002; SUN 2011; MOHAMED and AHMAD, 2014). Ti_3SiC_2 has a melting point equal 3000 °C due to the strong Ti-C-Ti-C-Ti covalent bond chains in the structure (ZHOU and SUN, 2000). Density of 4,53 g/cm^3, hardness ~ 4 GPa and elastic modulus ~ 320 GPa (TONG *et al*., 1995; BARSOUM and EL-RAGHY, 1996; EL-RAGHY and BARSOUM, 1999; EL-RAGHY and BARSOUM, 1996; GILBERT *et al*., 2000; ZHOU and SUN, 2000; YIN, ZHANG, and CHENG, 2011).

More than 45 years ago, Jeitschko and Nowotny were the firsts to synthesize Ti_3SiC_2 via chemical reaction between TiH_2, Si, and graphite at 2000 °C (JEITSCHKO and NOWOTNY, 1967). It is known that a pure single-phase Ti_3SiC_2 was synthesized by chemical vapor deposition in small quantities and by reactively hot pressing Ti, graphite and SiC powders at 40 MPa and 1600 °C (EL-RAGHY and BARSOUM, 1996; EL-RAGHY *et al*., 1997; GAO and MIYAMOTO, 1999). Nowadays studies have shown that Ti_3SiC_2 can be obtained by chemical vapor deposition, combustion synthesis, reactive sintering, hot isostatic pressing, arc-melting consecutive by annealing, thermal explosion, hot pressing and spark plasma sintering from the elemental powders (TONG *et al*., 1995; EL-RAGHY and BARSOUM, 1996; LIS *et al*. 1997; ZHOU and SUN, 2000; GAO *et al*., 2002; SUN *et al*., 2002; RADOVIC and BARSOUM, 2013; ABU, MOHAMED and AHMAD, 2014).

In the meantime, various attempts have shown that in synthesis of Ti_3SiC_2 what it is difficult to obtain is a single-phase product. This occurs due to the strait stable region of Ti_3SiC_2 in the ternary phase diagram of the Ti-Si-C system as represented in Figure 2 (WAKELKAMP, VAN LOO and METSELAAR, 1991; SAMBASIVAN and PETUSKEY, 1992; ARUNAJATESAN and CARIM, 1995; GAO *et al*., 2002). Studies have shown the presence of secondary phases as TiC, SiC or titanium silicide in synthesis of bulk Ti_3SiC_2 (EL-RAGHY *et al*., 1997). In their studies to synthesize pure Ti_3SiC_2, Barsoum *et al*. found less than 2 vol.% of SiC and TiC secondary phases via reactive hot pressing from 3Ti/SiC/C at 1600 °C, 40 MPa, for 4 h (EL-RAGHY and BARSOUM, 1996; GAO and MIYAMOTO, 1999; GAO *et al*., 2002). Another route showed two-step processes in which titanium, silicon and carbon powder or TiC, silicon and carbon mixture were first reacted together to form a powder compact that was subsequently pulverized and then hot pressed to yield polycrystalline samples. These procedures however led to mixtures of

Ti_3SiC_2; TiC_x, and $TiSi_2$ and sometimes $Ti_5Si_3C_x$, and/or SiC (EL-RAGHY and BARSOUM, 1999).

Figure 2- Ternary diagram of Ti-Si-C system at 1200 °C. (a) under 1 atm pressure and (b) under 240 MPa.

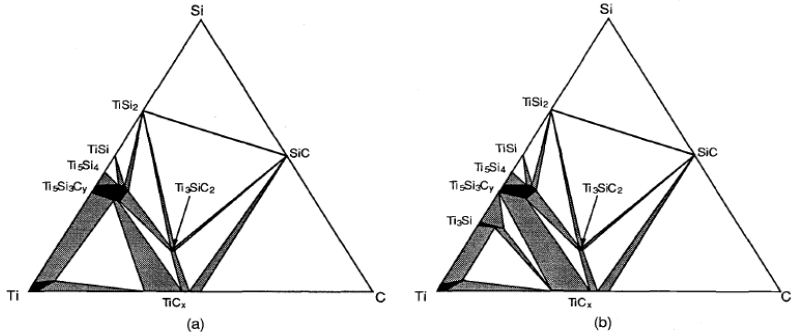

Source: (SAMBASIVAN and PETUSKEY, 1992; ARUNAJATESAN and CARIM, 1995)

However, the chosen route for the synthesis of this material will directly influence in the produced phases and its amount at the end of the synthesis. Lis and co-wokers synthesized samples with 80 vol% to 90 vol% Ti_3SiC_2 and TiC as secondary phase via combustion synthesis followed by hot isostatic pressing (PAMPUCH et al., 1989; LIS et al., 1995; MORGIEL, LIS and PAMPUCH 1996). Zhou *et al.* used an *in situ* HP solid-liquid synthesis of dense Ti_3SiC_2, resulting in ~ 92 wt% Ti_3SiC_2 (SUN, 2011).

With the multiphase presence in synthesis of Ti_3SiC_2, the properties of such systems are limited by the chemical interactions and formations of reaction products at the metal-ceramics interface (ARUNAJATESAN and CARIN, 1995). For example, the hardness can be significantly enhanced by the reaction of Ti_3SiC_2 with carbon to form TiC surface layers. Reaction with silicon, on the other hand, enhances the oxidation resistance and the surface hardness (EL-RAGHY and BARSOUM, 1998; EL-RAGHY and BARSOUM, 1999).

The temperature also has an influence on the properties of Ti_3SiC_2. At room temperature it is brittle. At high temperature it has plastic behavior with yield points of 300 MPa and 100 MPa in compression and flexure, respectively, and it undergoes a brittle-to-plastic transition

(BPT). At higher pressure they are quite plastic even in tension (EL-RAGHY and BARSOUM, 1999; RADOVIC and BARSOUM 2013).

Due to all those properties Ti_3SiC_2 can be used for civil and military applications. Furthermore it can be used in high temperature applications, such as sputtering targets for electrical contact deposition, turbine blades (Impact Coatings, Sweden) (RADOVIC and BARSOUM 2013), wear and corrosion protection, heat exchangers, components where rotating parts are used and low friction applications based on basal plane lubricity (SUN, 2011).

2.2. ADDITIVE MANUFACTURING

Additive manufacturing is the term, which presents a range of novel techniques that are capable to produce, layer by layer, accurate bodies with a desired geometric shape from a desired material with the aid of a computer-designed model with a small human intervention and without molds or die walls. In manufacturing cycles, prototypes are required in order to cognize form, fit and functionally of the design parts before higher investment. In order to remedy these needs and to reduce high cost and time consuming, these techniques appeared. It replaced the old manufacturing methods like skilled craftsman or skilled model makers from 2D engineering drawing, whom can take weeks, sometimes months to finish a prototype. It can lead to time saving of up to 90 % and the costs of production are reduced up to 70 %. (PHAM and GAULT, 1998; SINGH, 2010; FILBERT-DEMUT, 2012).

Additive manufacturing concept consists of building an accurate body by the addition of material by point, line or planar, layer-by-layer from the desired material with the aid of a CAD-program. The additive manufacturing is based on five general steps: First, a specific shape is created with the aid of a CAD-program (or with preferred animation modelling software). Second, conversion of a virtual CAD-model into a STL (standard tessellation language) file, which approximates the surface of the model by polygons. After that, the additive manufacturing software slices the virtual model (STL file) into cross-sections. Then a layer atop another the three-dimensional part is recreated. The last step consists in cleaning and removing of final material (SINGH, 2010; CHUA, LEONG and LIM, 2010; FILBERT-DEMUT, 2012).

Besides the ability to create physical models irrespective of their shapes and complexities directly from computer aided design (CAD) (SINGH 2010), time wasting reduction and lower costs, additive

technique offers a new product without tooling or confining surface, such as mold or die wall (TRAVITZKY *et al*., 2014).

Additive manufacturing was initially created to use polymer and other organic materials, but the research was extended to almost all variations of materials, including metals and ceramics (FILBERT-DEMUT, 2012). These techniques increased with the development of computer-aided design and manufacturing techniques (CAD/CAM) (SINGH, 2010; FILBERT-DEMUT, 2012).

A brief example of additive prototyping includes: (i) Selective Laser Sintering (SLS), where the powder from required material (commonly nonmetal) is shaped by a Laser sintering; (ii) Laminated Object Manufacturing (LOM), that consists in shaping by layers from adhesive-coated sheet material; (iii) Fused Deposition Modelling (FDM), where molten polymeric materials is deposited layer-by-layer by through thread by a movable nozzle; and (iv) the three-dimensional printing that will be discussed in the following item. (SINGH, 2010; FILBERT-DEMUT, 2012). The methods and major concepts of additive techniques are shown in Figure 3.

Figure 3 - General aspect of additive manufacturing techniques.

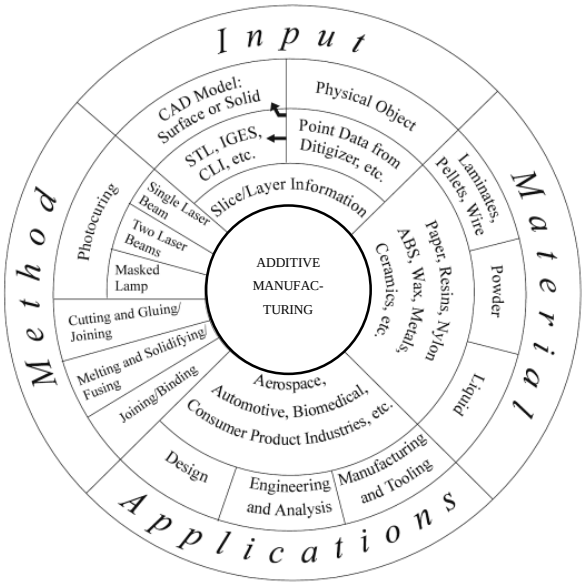

Source: (CHUA, LEONG and LIM, 2010).

2.2.1. Three-dimensional printing

Three-dimensional printing (3DP) belongs to the Additive Manufacturing techniques, in which the body is built layer-by-layer from the addition by point on/of the required material (CALI *et al*., 2012; TRAVITZKY *et al*., 2014). It was developed more than 30 years ago and beyond the advantages of the Additive Manufacturing techniques, 3DP can also produce precise parts with complex shape. It is flexible to all fields of materials. (DIMITROV, SCHREVE and BEER, 2006; SINGH, 2010; TRAVITZKY *et al*., 2014). It is based on ink-jet technology, which encompasses two approaches: direct and indirect ink-jet printing (TAY *et al*., 2003; TRAVITZKY *et al*., 2014).

Direct ink-jet printing method, also called Drop on Drop deposition method, consists in an ink composed by the desired material, which is printed onto a printing substrate (SLADE and EVANS, 1998; EDIRISNIGHE et al. 1999; EVANS, 2000; BLAZDELL, 2003; DIMITROV, SCHREVE and BEER, 2006; TRAVITZKY *et al*., 2014). In ceramic fields, for example, ceramic wax-based inks in a hot melted state can be deposited on a cold substrate for further solidification (SEERDEN et al. 2001; NOGUERA, LEJEUNE and CHARTIER, 2005; TRAVITZKY *et al*., 2014). Furthermore, ceramic suspensions can be printed and then dried due to the evaporation of the volatile solvent (RAMAKRISHNAN et al. 2005; TRAVITZKY *et al*., 2014). The bonding occurs by printing the ceramic suspension with volatile liquid on an absorbent substrate. This approach is capable to offer tailoring through blending and diluting ceramic suspension, leading to a graded composition quality, good surface and high dense parts of printed bodies (MOTT and EVANS 1999; TRAVITZKY *et al*., 2014). Since it allows producing dense ceramic parts, this is the only technique in additive processing that does not need required post-processing treatment (TSENG, LIN and WANG, 2006; TRAVITZKY *et al*., 2014). However, in direct ink-jet printing the variety of materials is limited (DIMITROV, SCHREVE and DE BEER, 2006).

Indirect ink-jet printing approach, known as Drop on Powder and Drop on Bed deposition too, consists in an ink composed by a binder solution that is printed directly onto a powder layer, bonding one layer to another until the body is completely formed (SLADE and EVANS, 1998; EVANS et al. 2003; DIMITROV, SCHREVE and DE BEER, 2006; TRAVITZKY *et al*., 2014). In this approach, the three-dimensional printer possess a spray head with a cartridge - which is responsible for depositing the binder solution - and two bays, one for powder feeding and

another for building, where the part is created. After receiving a command from CAD-program the spray head starts to deposit the binder solution onto the first powder layer. Once that the spray head moved across the two bays, it rolls over a new layer of powder from the feed bay to the build bay, and then the spray head deposits again the binder solution onto the new layer (Fig 4). This process is repeated until the final part is obtained (SUN, 2002).

Figure 4 - Representation of indirect ink-jet printing process.

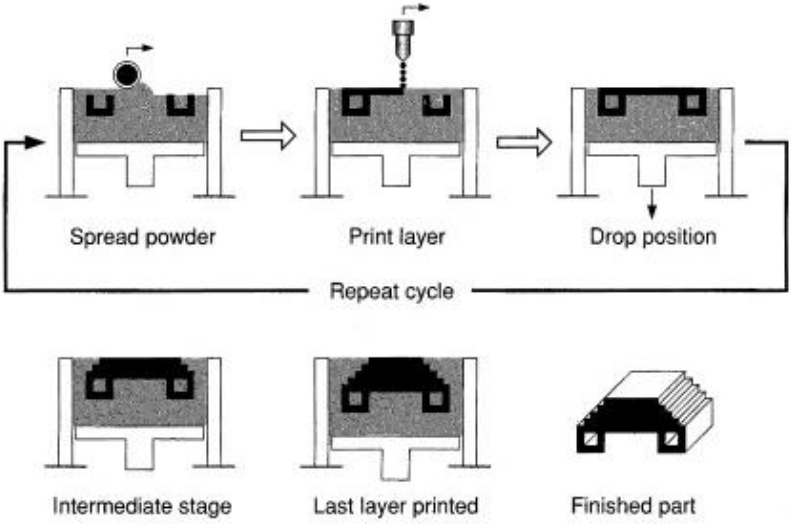

Souce: (JEE and SACHS, 2000)

This indirect ink-jet printing method is the most commercially used due to the high diversity of shape and powder material that is allowed to use (TRAVITZKY *et al*., 2014). However, post-processing treatments are required due to the high porosity that printed part show owing the density limitation on the distribution of dry powder (KARAPATIS, GRIETHUYSEN and GLARDON, 1998; SINGH, 2010; TRAVITZKY *et al*., 2014). In indirect ink-jet printing the properties of the final product are directly related to the properties of the material used, such as particle size, pourability, wetting behavior and processing parameter such as dimension and build orientation. For example, the higher the pourability of the material the higher will be the resolution and the thinner will be the

layers of the printed part. Materials with high size grain will offer higher porosity in final product (TRAVITZKY *et al*., 2014). Figure 5 illustrates ceramic parts fabricated by 3DP printing of both approaches.

Figure 5 - Printed ceramic parts via 3DP: (a) dental restoration, (b) impeller, (c) micro-pillar array, (d) bone implant, (e) macrocellular structures with versatile ligament lengths.

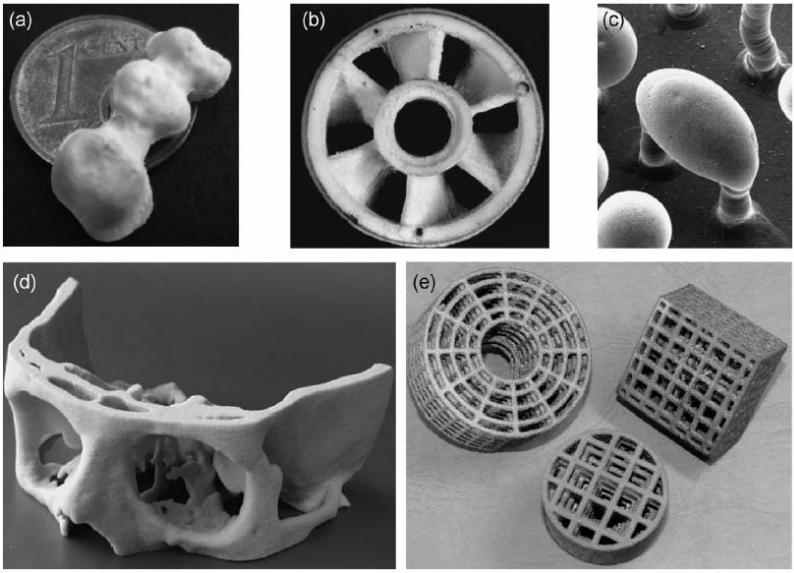

Source: (NOGUEIRA, LEJEUNE and CHARTIER, 2005; KHALYFA et al., 2007; SCHLIER et al.,2011; FU et al., 2013; TRAVITZKY et al., 2014)

Figure 6 shows a scheme of the 3DP technique. It has been applied to aerospace, automotive, coin making, tableware, biomedical etc. (SINGH, 2010) and has potential application in tissue engineering scaffolds and functional and advanced ceramic (TRAVITZKY *et al*., 2014).

Figure 6 - Representation of 3DP techniques.

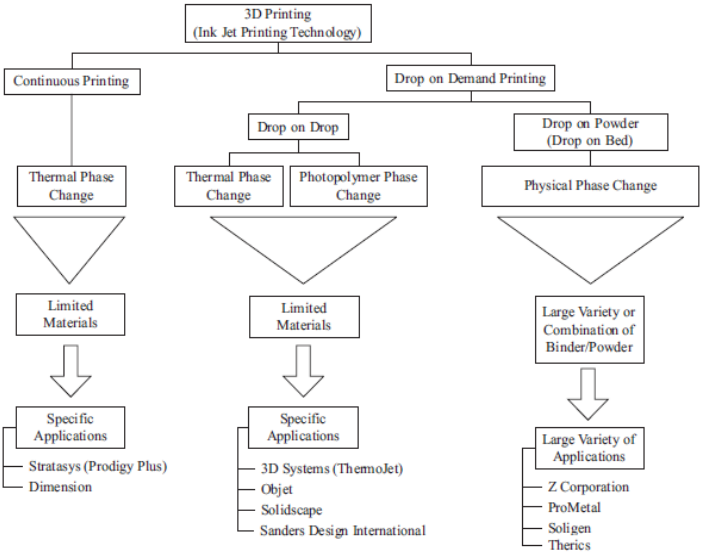

Source: (DIMITROV, SCHREVE and BEER, 2006)

2.3. PRESSING PROCESS

In ceramic field there are several forming methods including isotactic and uniaxial pressing, slip and taping casting, extrusion, etc. The choice of forming method will depend on the required properties of the final part and the raw material properties, such as product size and shape, surface quality and microstructural characteristic (REED, 1995). Furthermore, the properties of shaped part – as packing homogeneity, sufficient strengths, geometrical tolerances and lower variations of density - can influence the properties after post-treatments, as handling, debindering and sintering (RIEDEL and CHEN, 2012). In case of sintering as a post-treatment, Shui *et al*. studied the influence of particle orientation and non-uniform packing density of elongated and spherical particle of alumina compacts by uniaxially and subsequent isostatic pressing before sintering. The study shows that for elongated shapes of alumina the particle orientation occurred during the uniaxial pressing

leads to anisotropic sintering shrinkage. In the case of spherical particle shape did not show the same results (SHUI *et al.*, 2001).

In pressing process the powder or granular ceramic is confined inside a rigid die or a flexible mold where the compaction and shaping occurs at the same time. Dry pressing arrived with the advantage to produce parts ranging widely in size and shape to close tolerances and essentially no drying shrinkage (REED, 1995). Beyond that, this technique is the most used in industry, owing the high efficiency and productivity with the goal of convert loose powder into a green compact part with maximum overall density and desired geometry. Dry pressing also encompasses two deviations: uniaxial and cold isostatic pressing (RIEDEL and CHEN, 2012).

2.3.1. Uniaxial Pressing

Uniaxial pressing is a significant forming process, which has the aim to compact a ceramic powder between rigid punch faces and die walls. This technique occurs in three mainly steps, (i) die filling, (ii) compaction and (iii) ejection of the compact parts. It involves two alternatives to compact a loose powder; at first through a single-action compaction, where only one punch exerts pressure on the die filled. Second, double-action pressing where both punches make pressure to compact the loose powder (Fig 7) (CHUA, LEONG and LIM, 2010; RIEDEL and CHEN, 2012).

Figure 7 - Single and double-action compaction in uniaxial pressing.

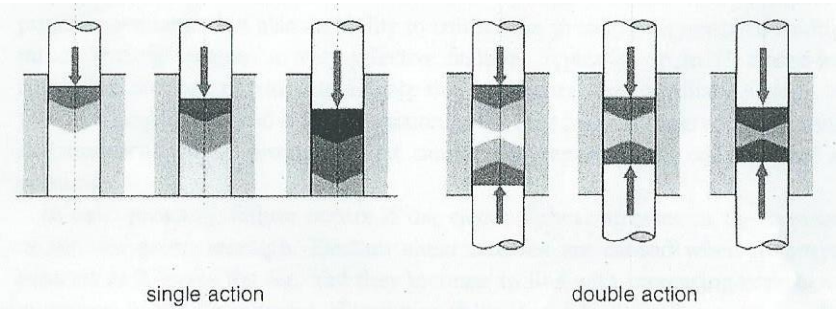

Source: (RIEDEL and CHEN, 2012)

Unsymmetrical density gradient is the higher disadvantage of single-action pressing, mainly due to wall friction effects leading in a warping (Anisotropic shrinkage) of the compact ceramics during the sintering (SHUI et al. 2001). This occurs owning the decreasing density from the top to the bottom of the compact part. However, in double-action pressing this drawback is remedied due to the pressure from both punches, i.e. the pressure is symmetrical to the central cross-section, causing a neutral axis (RIEDEL and CHEN, 2012). The restrictions of uniaxial pressing are parts with features perpendicular to the pressing direction that cannot be compacted and stripped (RIEDEL and CHEN, 2012).

The uniaxial press can be hydraulic and mechanical (REED, 1995). The presented technique allows creating structural, electronic, magnetic and refractory parts (RIEDEL and CHEN, 2012).

2.3.2. Cold Isostatic Pressing

Cold Isostatic pressing (CIP) is a process where densification occurs under an isostatic or near-isostatic pressure condition. In this method, an elastomeric mold is used to seal the powder and then the pressurization occurs by a liquid with hydrostatic pressure (RIEDEL and CHEN, 2012). The greatest advantage is that compaction occurs in all directions uniformly, promoting a uniform density of the CIPed part and no pressing defects in ejection stage when compared to uniaxial pressed parts (AZOM.COM, 2013; RIEDEL and CHEN, 2012).

Two approaches comprise CIP, wet-bag and dry-bag isostatic pressing. Dry-bag isostatic pressing involves a flexible membrane located inside the pressure vessel used during pressing cycles in order to separate the pressure fluid from the mold. Figure 8 shows the four steps involved in dry-bag process.

Figure 8 - Mechanism step by step of production of spark plug insulators via dry-bag pressing.

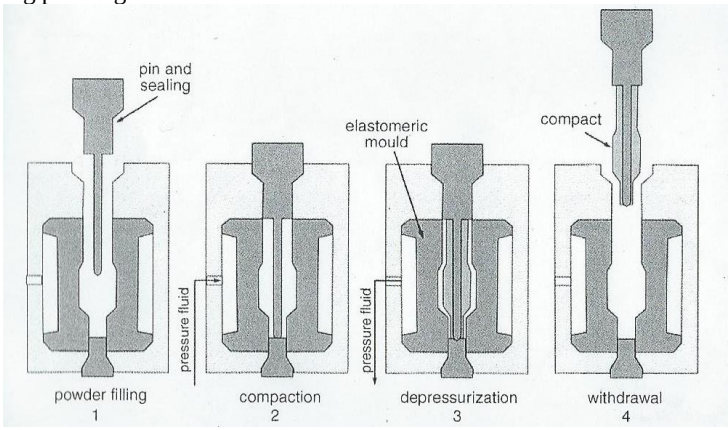

Source: (RIEDEL and CHEN, 2012)

In step one the mold is filled with powder. In step two the hydrostatic pressure occurs due to the pressurization of the pressing fluid (radially). The releasing pressure is characteristic of step three when the mold deforms back to its initial shape. The last contains the withdrawal of the compacted part by lifting the core rod. (REED, 1995; RIEDEL and CHEN, 2012)

This method is required for mass production processes and is usually required for pressing small elongated parts, as spark plug insulators, milling and bearing balls, crucibles and thermocouple protection (REED, 1995; RIEDEL and CHEN, 2012).

In wet-bag isostatic pressing an elastomer mold is filled with the desired powder, sealed and placed into the pressure vessel (Fig 9). The vessel is closed and then filled with an aqueous suspension for hydrostatic pressurization (RWTH Aachen University - Institute of Mineral Engineering). To avoid defects caused by the expansion of the elastomeric mold, a controlled depressurization is needed (CHUA, LEONG and LIM, 2010; RIEDEL and CHEN, 2012).

Figure 9 - Scheme of wet-bag isostatic pressing process: (a) filling, (b) loading, (c) pressing, and (d) despressurization prior to removing part.

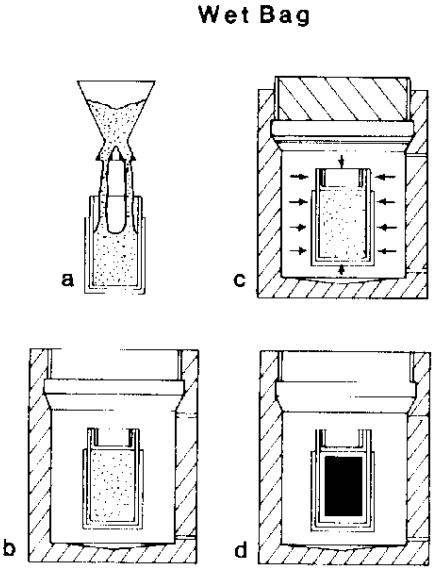

Source: (REED, 1995)

Synthetic and silicone rubber, polyvinyl chloride (PVC) and polyurethane are suitable to use as elastomers bag materials. With the aid of this elastomeric mold wet-bag CIP can be used for complex shape, large volume and elongated dimensions (REED, 1995).

CIP provides a uniform shrinkage of green bodies, consequently avoiding anisotropies in green CIPed samples (RWTH Aachen University - Institute of Mineral Engineering). Furthermore, greater green strength and consequently higher reproducible sintering shrinkage of the isostatically pressed parts is owing to the homogeneous density that this method is able to provide. Other advantages include: absence of ejection step, low tooling cost and the possibility to avoid die wall lubricants (RIEDEL and CHEN, 2012).

CIP is popular for densification ceramic powder without the use of pressing aids. It can also be applied for re-pressing of green parts previously shaped by either axial pressing or by other forming processes

with the aim to increase the density and the homogeneity of density distribution (RIEDEL and CHEN, 2012).

The isostatic pressing advantages consist in capability to process immiscible systems, capability to process composites covering high-melting point materials. Furthermore, diffusive alterations can be avoid by choosing the proper pressure-temperature-time cycle, possible to produce a fine-grained material with a uniform microstructure. Complex geometries can be made to near-net shape and for arbitrarily powder mixture an isotropic composite can be reached (TURNER and ASHBY, 1996).

2.4. SINTERING

Firing systems are characteristic of thermal treatment in which compact green bodies are submitted with the aim to develop its properties and microstructure. Sintering corresponds to the second step of firing systems, which have the purpose to consolidate the part during the firing. The first and third step of firing system correspond to preliminary reactions and cooling (REED, 1995).

Sintering corresponds to a process where interparticle pores in a powder material are removed due to the atomic diffusion through capillary forces (CHEN and WANG, 2000). Thus, it commonly implies in densification and shrinkage of ceramic parts. It can be defined by the combination of pore removal, retraction of the part and growth and formation of strong bonds between adjacent particles. Sintering usually begins after one-half to two-third of melting temperature of the product, what is enough to cause atomic diffusion or viscous flow (REED, 1995).

The driving force of sintering is given by the reaction of the surface area due to the replacement of a loose powder with high surface energy (solid-vapor) to a solid connected by grain boundaries with lower energy. However, properties of the green compact - as composition, density, porosity and particle shape – and sintering parameters – as atmosphere, pressure, temperature and heating and cooling rate – will control the process inside the compact parts (LEE, 1994).

Figure 10 exemplifies the four general stages involved in the solid-state sintering. First stage shows the powder in the beginning of the process. The second stage is called initial stage of sintering and consist in the particles rearrangement and neck formation in the point of particles contact. Densification in this initial stage is approximately 10 %. In the third stage, which is called intermediate stage, the necks increase and

porosity decreases considerably. Shrinkage occurs, grain boundary starts and it growths slowly. In this stage the relative density can reach 90 % (LEE, 1994). In the final stage the pores are eliminated and the grain size increases.

Figure 10 - Stages of Sintering Process. (a) Loose powder, (b) initial stage, (c) intermediate stage and (d) final stage.

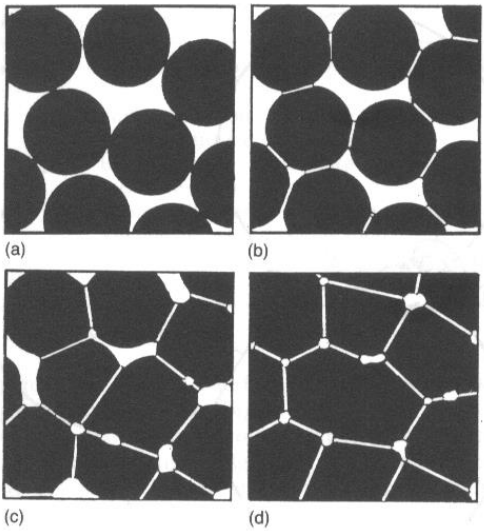

Source: (LEE, 1994)

The mass transport mechanism evolved in sintering are surface diffusion, evaporation-condensation, boundary diffusion, lattice diffusion, viscous flow and plastic flow (REED, 1995).

3. EXPERIMENTAL

3.1. RAW MATERIALS

For the feedstock mixture Ti_3SiC_2 powder (Beijing Jinhezhi, Material Co, Ltd, Bejing, China) and dextrin (Dextrin Superior Gelbmittel, Südstärke GmbH; Schrobenhausen, Germany) as binder were used. The chemical composition and characteristics of feedstock material are presented in Table 1.

Table 4 - Chemical composition, d50 and melt temperature of feedstock materials.

Materials	Chemical Composition	d_{50}[µm]	T_m[°C]
Ti_3SiC_2 powder	Ti_3SiC_2 (2 wt% TiC, Ti_5Si_3)	3	3000
Dextrin	$(C_6H_{10}O_5)_n$, n = 10-200	100	>2300

3.2. EXPERIMENTAL PROCEDURE

All the steps involved in the fabrication of Ti_3SiC_2-based composites are shown in Figure 11. The general steps are Ti_3SiC_2 and dextrin powder mixture preparation, three dimensional printing, cold isostatic pressing, uniaxial pressing and sintering.

Figure 11 - scheme of experimental procedure.

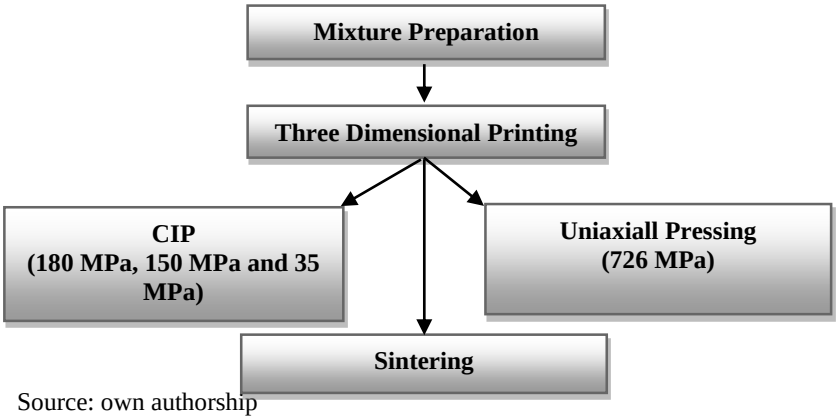

Source: own authorship

3.2.1. Mixtures Preparation

The commercial Ti_3SiC_2 powder had the initial particle size of ~ 12 µm. To achieve a smaller particle size, commercial Ti_3SiC_2 powder were first milled in ethanol for 4 hours and 1500 rpm in an agitator ball mill and then dried a vacuum. The milled powder achieved a particle size of ~ 3 µm and were first blended with 10 wt% dextrin. Prior the mixture, dextrin was sieved to 100 mesh and dried for 24 h in 70 °C to avoid agglomeration. Dried dextrin and milled Ti_3SiC_2 powder (~ 3 µm) was mixed for 48 h in a ball mill. The blended powder was sieved again to 100 mesh and then dried for 24 h in 70 °C before three-dimensional printing. Dextrin was used with the aim to bind the Ti_3SiC_2 powders thus assisting the 3DP performance.

3.2.2. Three Dimensional Printing

Rectangular samples were designed by a CAD-software (SolidWorks 2010, Dassault Sistêmes SolidWorks Corp, Concord, USA) with dimensions of 50 x 7 x 6 mm^3, and for printing an indirect 3D printing system (ZPrinter® 310, Z Corporation, Burlington, USA) was used. A printer solution composed of 1:7 vol ratio of glycerin and distilled water was injected into the Ti_3SiC_2-blended powder bed. The thickness layer were adjusted to 0.1 mm and binder saturation of 50 % and 100 % Core and Shell, respectively. It were printed approximately 6 sets of rectangular samples. In which, each set contained eleven rectangular samples. After printing the samples, it were left in powder bed for drying at room temperature for 24 h and then dried at 70 °C for 24 h.

3.2.3. Cold Isostatic Pressing (CIP)

After three dimensional printing the samples blended with 10 % of dextrin containing fine Ti_3SiC_2 were divided in 3 sets (Fig 11). One set was directly sintered, another one was uniaxial pressed before sintering and the last set was subdivided in another 3 sets, which were submitted to cold isostatic pressing prior to sintering, but with different pressures (180 MPa, 150 MPa and 35 MPa).

For CIP, green samples were first vacuumed encapsulated in a latex bag and then a second time encapsulated in an aluminum bag. Posteriorly the three subdivided sets of samples were separated and submitted to a pressure of 180 MPa, 150 MPa and 35 MPa, for each set, respectively.

All sets were under pressure for 30 seconds in an isostatic wet bag press machine (LOOMIS PRODUCT Kahlefelg GmbH, Kaiserslautern) with 7.41 L of a mixture of 95 % water and 5% water soluble oil.

3.2.4. Uniaxially Pressing

The green printed samples were first sanded by using a polished paper of 320 µm, until they reached the necessary size to fit in the uniaxial mold, equivalent to 6 x 50 mm^2. The specimens were subjected to a pressure equal to 726 MPa for 30 seconds (Paul Otto Weber GmbH, Remshalden, Germany).

3.2.5. Sintering

To achieve dense composites sintering was required. Samples were first placed in alumina crucible and then placed in an alumina tubular furnace (HTRH 1000-300/18 GERO-Hochtemperaturöfen GmbH, Neuhausen, Germany) at 1600 °C with a dwell time of 2 h performed in flowing argon atmosphere. The heating and cooling rate equals 180 K/h.

3.3. CHARACTERIZATION AND ANALYSIS METHODS

3.3.1. Thermal Analysis

Thermogravimetric analysis (TGA) and differential thermal analysis (DTA) was required to investigate the decomposition of dextrin powder and Ti_3SiC_2-based composites (dextrin and Ti_3SiC_2) after printing. The measurements were carried out in flowing argon with a heating hate of 5 K/min.

3.3.2. Density and Porosity

For each step involved the density and porosity were measured, i.e. after the three-dimensional printing, pressing process and sintering. Open porosity was obtained through the equation (1).

$$\text{Popen} = \left(1 - \left(\frac{\rho\text{geo}}{\rho\text{th}}\right)\right).100 \quad (1)$$

Where,

P_{open} = open porosity (%);
ρ_{geo} = geometrical density (g/cm3);
ρ_{th} = theoretical density (g/cm3).

The theoretical density is obtained with a helium pycnometer (Accupyc 1330 Micromeretics, Norcross, USA) and the geometrical density is the ratio of the mass (m) and volume (V) of the samples.

Archimedes methods were also used to determine density. The real density (φ) is obtained by Archimedes methods as presented in equation 2. For Archimedes methods, samples are first weighed dry and then they are immersed in water and weighed again.

$$\varphi = \frac{m1}{(m1-m2)} \cdot \varphi H_2O \quad (2)$$

Where,

$m1$ = dry mass (g);
$m2$ = mass of sample immersed (g);
φH2O = density of water in the temperature during the measurement (g/cm^3).

3.3.3. Dimensional changes (Shrinkage)

The dimensional changes were also calculated for each steps involved in this work. Change in length (Δy), width (Δx), height (Δz) and volume (ΔV) was determined by the following equation.

$$\Delta x = \frac{\text{X initial} - X\,final}{Xinitial} \times 100 \quad (3)$$

3.3.4. Phase Analysis

In order to analyse the structure of green and sintered samples X-ray diffraction technique (Kristalloflex D500, Siemens, Karlsruhe, Germany) was used. The diffraction angle (2Θ) was measured in a scanning rate of 1.2 °/min in the range of 10 ° to 70 ° with Cu-Kα radiation.

3.3.5. Microstructure Characterization and Elemental Analysis

Microstructure of green and sintered samples were analyzed by scanning electron microscopy (SEM; Quanta 200, FEI, Praga, Czech Republic) and the phase's chemical composition defined by Energy-dispersive X-ray spectroscopy (EDX, INCA x-sight TVA3, Oxford Instruments, Oxford, Great Britain). All samples were analyzed using the polished cross section.

3.3.6. Young's Modulus

For v determination of Young's Modulus of sintered samples the propagation time of an ultrasonic measuring device was measured (Krautkrämer GmbH, Hürth,Germany), according to DIN EN 843-2 (DIN EN 843-2, 2007). The resonance peaks in horizontal and vertical directions of the samples were measured as showed in equation (3) and (4).

$$E\mathrm{h} = \varphi \cdot \left(\frac{l}{th}\right)^2 \cdot \frac{(1+\nu).(1-2\nu)}{1-\nu} \quad (3)$$

$$E\mathrm{v} = \varphi \cdot \left(\frac{l}{th}\right)^2 \cdot \frac{(1+\nu).(1-2\nu)}{1-\nu} \quad (4)$$

Where,

$E\mathrm{h}$ = young's Modulus in horizontal direction (MPa);
Ev = young's Modulus in vertical direction (MPa);
l = length of sample (mm);
h = height of sample (mm);
th = resonance peak in horizontal direction (μm);
tv = resonance peak in vertical direction (μm);
ν = Poisson ratio (0.2);

φ = real density (g/cm^3).

3.3.7. Flexural Strength

A four- point bending setup (DIN EN 843-1, 2008) was required to obtain the flexural strength by using an Instron 5565 testing machine (Instron Corp., Carton, USA). A crosshead speed of 0.5 mm/s and with span lengths of 10 mm (load) and 20 mm (support) was used. To avoid stress peaks at the rim, the edges of the tensile surface of the samples were deburred manually. From equation (5), it was possible to obtain the flexural strength.

$$\sigma = \frac{3 \cdot F \cdot d}{b \cdot h^2} \quad (5)$$

Where,

F = maximum load (N);
d = average distance between the axes of support and load span (mm);
b = width of specimen (mm);
h = height of specimen (mm).

4. RESULTS AND DISCUSSION

4.1. THERMAL ANALYSIS

Figure 12 shows the thermogravimetric and differential thermal analysis of dextrin in argon. The first decomposition starts around 70 °C corresponding to the dehydration, once dextrin has affinity towards water. The decomposition of dextrin occurs approximately at 250 °C and the amorphous carbon residue is about 42 wt %. The weight fraction of dextrin in powder blends is 10 wt%, thereby after 600 °C the amount of carbon content in the specimens is 4.2 wt %.

Figure 12 - Weight loss of dextrin in function as temperature.

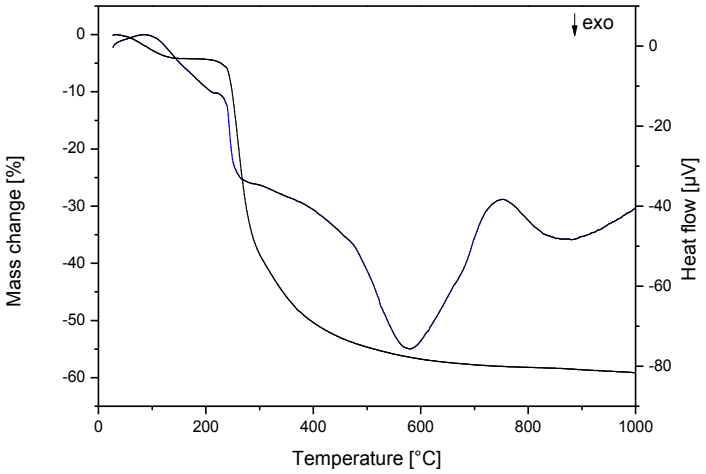

The endothermic peak around 90 °C is assigned to evaporation of water. Exothermic peaks at 263 °C, 580 °C and 872 °C are related to the first and second decomposition and a phase change of dextrin, respectively (VEIGA et al. 2002).

Figure 13 shows the thermogravimetric analysis curve of Ti_3SiC_2-based composites after three-dimensional printing in argon atmosphere. Ti_3SiC_2 proved to be stable up to 1300 °C under Argon atmosphere (RACAULT *et al*., 1994), thus concluding that until approximately 1300 °C occurs only the decomposition of dextrin (Fig. 12).

Figure 13 - Weight loss of Ti_3SiC_2-based composites as function of temperature.

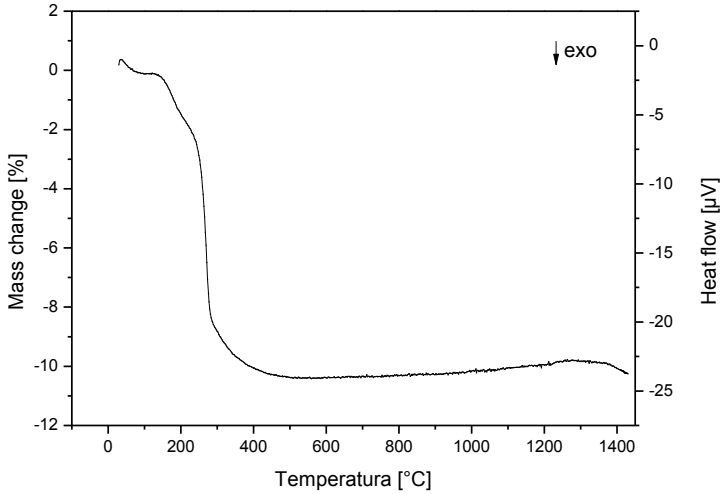

The degradation of dextrin in samples after three-dimensional printing starts around 40 °C corresponding to absorbed water by dextrin. Decomposition of dextrin starts to occur around 130 °C. Above approximately 467 °C the mass change reaches a plateau with a constant residue value of 90 %. As predicted in literature, above 1300°C a weight loss starts, implying the decomposition of Ti_3SiC_2 (RACAULT *et al.*, 1994; BARSOUM and EL-RAGHY, 1996).

4.2. MASS AND DIMENSIONAL CHANGES

As previously stated after three-dimensional printing the Ti_3SiC_2-dextrin specimens were divided in 3 sets (Fig 11). One set was directly sintered, another was uniaxial pressed at 726 MPa before sintering and the last set was subdivided in another 3 sets, which were submitted to cold isostatic pressing prior of sintering, but at different pressures (180 MPa, 150 MPa, and 35 MPa).

Figure 14 exhibits the mass change for all samples after sintering. CIPed samples before sintering at 180 MPa, 150 MPa, and 35 MPa presented weight loss of 11 %, 12.4 %, and 11.3 %, respectively. Samples uniaxially pressed before sintering present 12.1 % of weight loss and

specimens without pressing process show a higher weight loss, equal 16.6 %.

Figure 14 - Mass change after sintering at 1600 °C

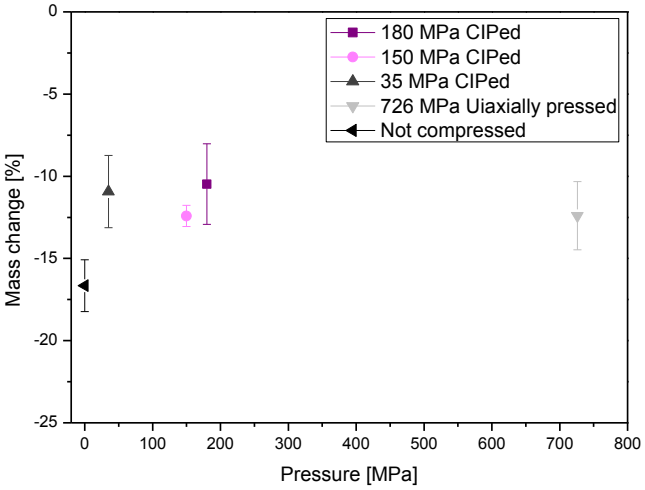

For all the samples a value of 5.8 wt% of the total weight loss corresponds to the decomposition of dextrin, which can be observed in TGA of Figure 12. The remaining values of weight loss to samples CIPed at 180 MPa, 150 MPa and 35 MPa are 5.2 %, 6.6 % and 5.5 %, respectively. For uniaxially pressed samples the weight loss equals 6.3 % and 10.8 % for samples without pressing before sintering. Those values can be associated to the vaporization of Si during the heat treatment due to the decomposition of Ti_3SiC_2 and therefore weight loss (RACAULT *et al.*, 1994; EL-RAGHY and BARSOUM 1997). At high temperatures the MAX Phases do not melt congruently but decompose practically to A-rich (Si-rich) liquids and $M_{n+1}X_n$ (Ti_2C) carbides or nitrides. Thermal decomposition occurs by the loss of the A (Si) element and the formation of higher–containing MAX Phases and /or MX (TiC) (RADOVIC and BARSOUM, 2013).

Figure 15 shows the linear shrinkage in direction x, y, z, and volumetric shrinkage after the pressing process for all samples. The samples that were CIPed at 180 MPa, 150 MPa, 35 MPa and uniaxially

pressed show linear shrinkage of 11 %, 22 %, 14 % and 23 %, respectively.

After pressing the volumetric shrinkage observed is 42 %, 46 %, 37 %, 65 % for samples that were CIPed at 180 MPa, 150 MPa and 35 MPa and uniaxially pressed, respectively.

Figure 15 - Shrinkage of pressed samples.

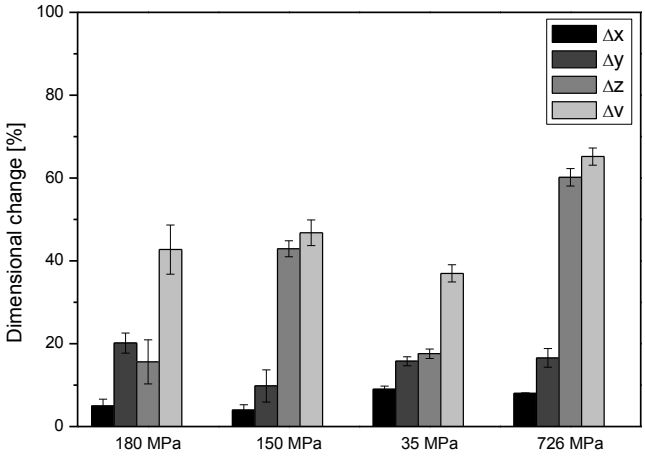

After sintering the samples show a higher linear shrinkage (Fig 16). The linear shrinkage for samples that were CIPed at 180 MPa, 150 MPa, 35 MPa, uniaxially pressed and without pressing before the sintering are 14 %, 24 %, 15,5 %, 8 % and 20 %, respectively. As stated in the literature, the shrinkage for pressed samples is higher than the samples without pressing before sintering; suggesting that a considerable amount of porosity may be retained in samples without pressing process (SUN *et al.*, 2002a). Another explanation may be due to the fact that samples that were not exposed to pressing before sintering may have occurred the burnout of binder, thus leading to a porous structure (SUN *et al,*. 2002a; SUN *et al,*. 2002b). The higher linear shrinkage value for CIPed samples can be explained by the fact that isostatic pressing provides a homogeneous density distribution, responsible for a higher value of

sintering shrinkage compared to uniaxial pressing (RIEDEL and CHEN, 2012).

Figure 16 - Shrinkage of sintered samples at 1600°C.

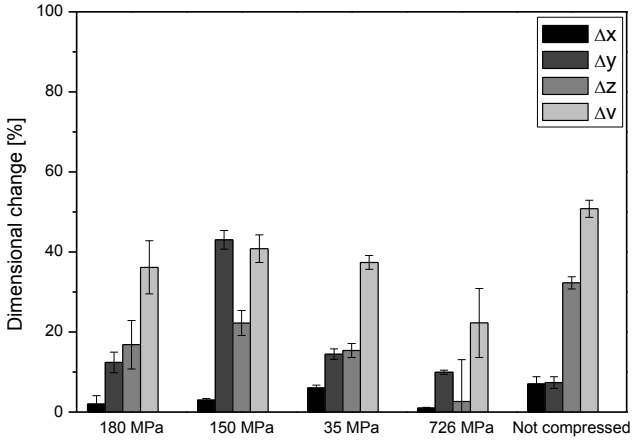

The volumetric shrinkage observed for the samples CIPed at 180 MPa, 150 MPa, 35 MPa, uniaxially pressed and not pressed after sintering is 36 %, 41 %, 39 %, 23 % and 51 %, respectively. In both steps (pressing and sintering) the average of volumetric shrinkage is positive, indicating the elimination of pores (SUN *et al*., 2002).

4.3. POROSITY DEVELOPMENT

The porosity involved in all steps of this work is presented in Figure 17. Initial porosity for green samples equals 68 %. After pressing process porosity decreases to 29 % for CIPed 180 MPa, 37 % for CIPed 150 MPa, 44 % for CIPed 35 MPa and 17 % for uniaxially pressed samples, in total, with pressing process a decrease of 24 % to 51 % in initial porosity can be reached. After heat treatment, as expected, all samples had a reduced porosity.

Samples that were first CIPed with 180 MPa, 150 MPa and 35 MPa and then sintered exhibit a final porosity of 3.6 %, 5.2 % and 13 %, respectively. Samples that were previously uniaxially pressed show 1.75 % porosity and specimens that were not submitted to compressing

exhibit the highest porosity, of 48 %. These values agree with the explanation given in the previous section, which suggests that porosity may be retained in samples without pressing process.

Figure 17 - Porosity involved in all stages of processing

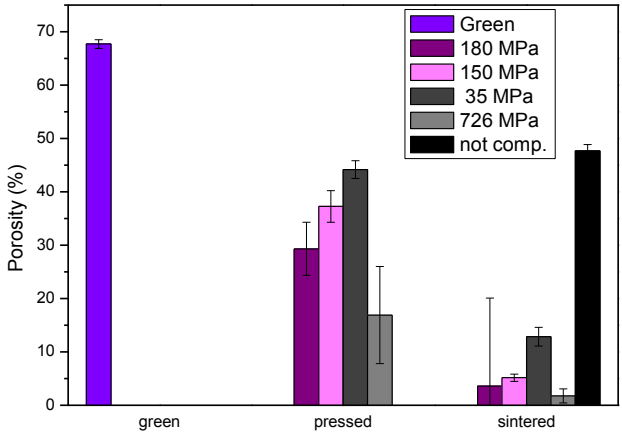

For samples that were not pressed and CIPed with 35 MPa before sintering, the value of porosity after sintering shows that the samples may not be appropriate for structural applications, once functional ceramics commonly have a need of porosity below 10 % (SUN *et al.*, 2002a).

The results presented for samples CIPed with 180 MPa and 150 MPa before sintering show that the cold isostatic pressing is a good alternative to compact green samples and reach high porosity, since the porosity after CIP decreases in a range of 24 % to 39 %. In the meantime, the process involving pressing and sintering was not able to achieve fully dense structure with density higher than 99 %.

These results content with Sun *et al.*, (2002), who studied the fabrication of three-dimensional Ti_3SiC_2 structures by three stages: three-dimensional printing, cold isostatic pressing and sintering processing. The layer thickness was in a range of 0.0035 in to 0.007 in.; saturation of binder in a range of 2 % to 40 % - Shell/core, and the concentration was varied in 10 %, 20 % and 30%. The powder used for fabrication of Ti_3SiC_2 structure was an as-synthesized powder from titanium, graphite (carbon)

and silicon carbide obtained by reactive hot pressing. The results for all samples with 10 %, 20 % and 30 % binder concentration showed an increase in porosity after cold isostatic pressing, however after sintering the density is higher than 99 % (SUN *et al.*, 2002a, SUN *et al.*, 2002b).

4.4. PHASES ANALYSIS

The X-ray diffraction analysis for milled Ti_3SiC_2 provided the diffraction scan exposed below (Fig 18). The feedstock powder for fabrication of Ti_3SiC_2-based structure presents the main phase Ti_3SiC_2, but also secondary phases like $TiSi_2$ and $Ti_{5.7}Si_{3.5}$.

Figure 18 - Diffraction scan of milled Ti_3SiC_2.

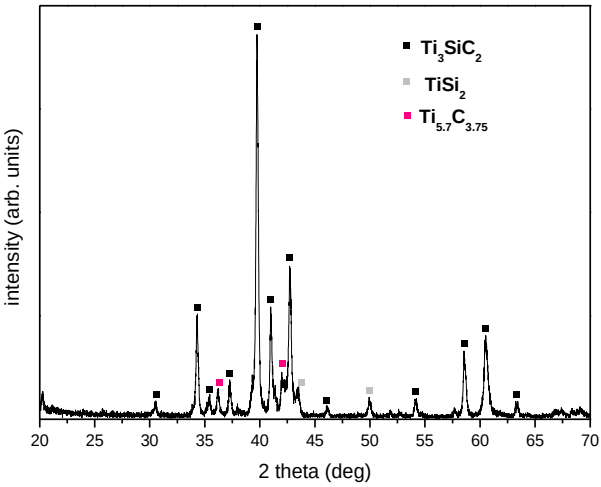

X-ray diffraction analysis for samples after sintering provided the diffraction scan exposed in Figure 19. As desired, the common phases in all samples after sintering are Ti_3SiC_2 and also Ti_8C_5. $TiSi_2$ is provenience from feedstock material and C from dextrin.

Figure 19 - Diffraction scan of samples after sintering process.

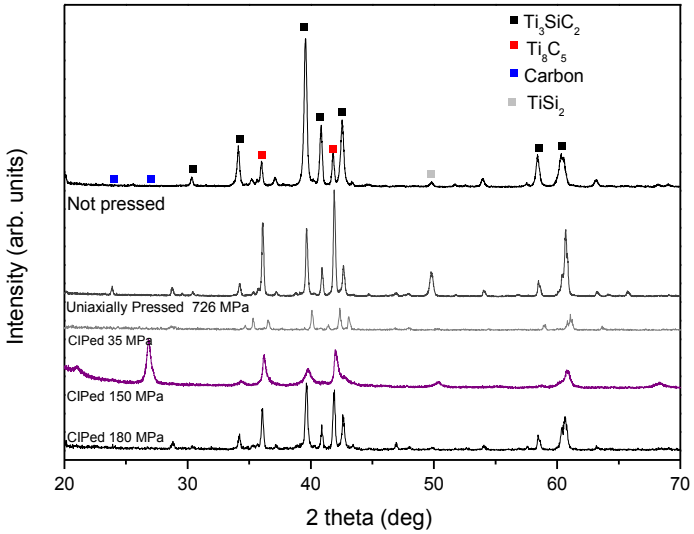

Samples CIPed at 150 MPa show a peak equivalent to carbon. The same behavior occurs to samples that were uniaxially pressed. The presence of carbon suggests low reactivity between Ti_3SiC_2 and dextrin. According to the literature, carburization kinetics in full dense samples is at least one order of magnitude slower than the porous compacts (EL-RAGHY and BARSOUM, 1997). The higher amount of weight loss (12.4 % e 12.1 % for CIPed at 150 MPa and uniaxially pressed, respectivamente) for these samples pressed confirm the non-reactivity between MAX Phase and carbon (discussed in section 4.5).

4.5. MICROSTRUCTURE CHARACTERIZATION

By using the scanning electron microscopy it is possible to analyze the microstructure in all stages of the process. Figure 20 presents the microstructure of a green sample with 68 wt% of porosity. In the scanning electron microscopy it is possible to notice the homogeneous microstructure and the pores (dark regions) in Ti_3SiC_2-based structure.

Figure 20 - Microstructure (1000x magnifications) of Ti_3SiC_2 blended with 10wt% of dextrin after three dimensional printing.

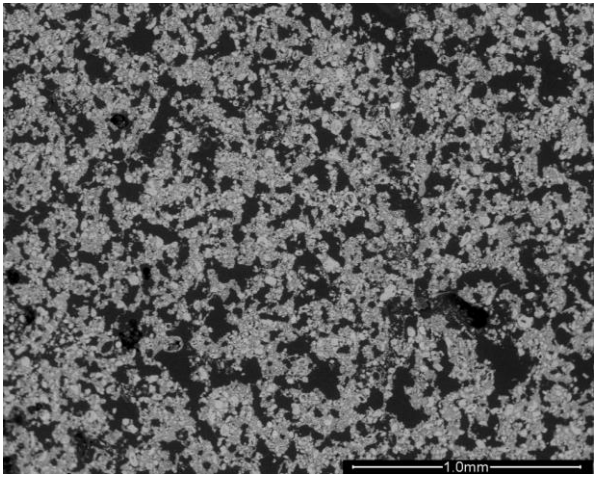

The microstructure of the samples after sintering is presented in figure 21. It is possible to observe that samples without pressing before sintering (Fig 21 (e)) present longer voids (dark region), agreeing with the explanation given in section 4.3, that related that samples without pressing process before sintering have a higher porosity, and this may be explained by two facts. On the one hand, the porosity may be retained in the samples structure and on the other hand, samples that were not exposed to pressing before sintering may occur the burnout of binder, thus leading to a porous structure. It is possible to note in Figure 21 the difference of porosity between samples. For samples that were submitted to pressing before sintering, the higher porosity belongs to samples that were CIPed with 35 MPa (44 %), as stated in Figure 20 (c). It also shows that uniaxially pressed samples (Fig 21 (d)) have lower porosity, nevertheless they also show crack formation.

Figure 21 - Microstructure after sintering at 1600 °C (50 x magnification). (a) CIPed 180 MPa ; (b) CIPed 150 MPa; (c) CIPed 35 MPa; (d) uniaxially pressed 726 MPa and (e) not compressed.

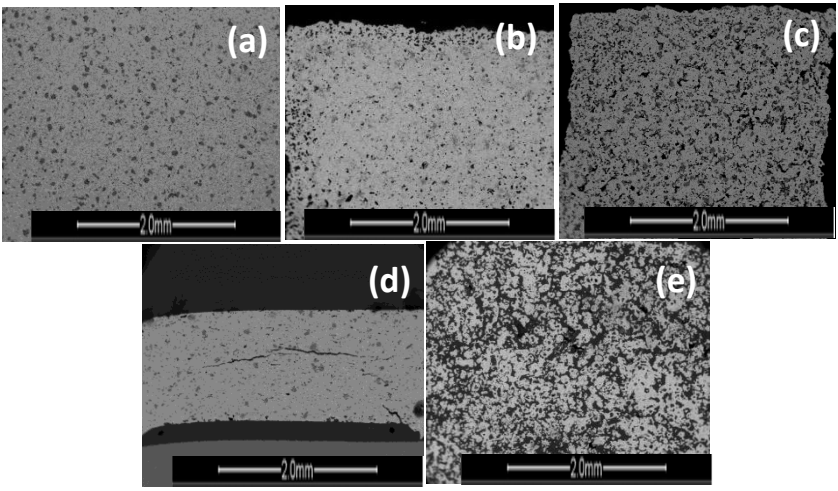

In disagreement with X-ray diffraction analysis the energy dispersive spectroscopy (EDS) shows presence of SiC in all samples (Fig 22). This event may have occurred due to the non-homogeneous way that SiC is distributed in the samples. As long X-ray diffraction is a specific analysis in only one spot of the samples this could hamper the detection of phases with small amount or/and non-homogeneous distributed. Another justification for the nonappearance of SiC peaks in X-ray diffraction analysis is caused by poor data from X-ray apparatus, thus leading to peaks of SiC and TiC overlapping since this is a qualitative and not quantitative analysis.

Figure 22 - Microstructure after sintering at 1600 °C (100 x magnification). (a) CIPed 180 MPa ; (b) CIPed 150 MPa; (c) CIPed 35 MPa; (d) 726 MPa and (e) not compressed

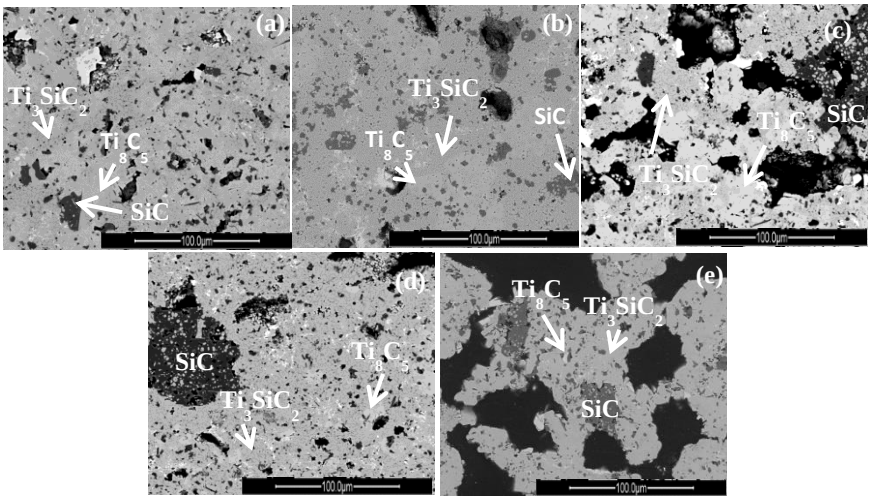

According to El-Raghy and Barsoum (1998) the Ti_3SiC_2 in contact with graphite can react and generate TiC_x by two reaction mechanism:

$$Ti_3SiC_2 + (3x-1)\,C = 3TiC_x + SiC \quad (1)$$

$$\Delta V \approx 12{,}2\ \%$$

$$Ti_3SiC_2 + (3x-2)\,C = 3TiC_x (x > 0.8) + Si \quad (2)$$

$$\Delta V = -15{,}7\ \%$$

Their experiments were carried out in vacuum furnace (10^{-3} Pa) at 1400 °C, 1500 °C and 1600 °C. Coupons of Ti_3SiC_2 synthesized from Ti and SiC powder by cold and hot pressing, placed between graphite foils as a sandwich, and the diffusion time was at a range of 1 h to 16 h. The results from X-ray also show no presence of SiC, according to this work. However for his studied EDS analysis also point the absence of SiC,

indicating the occurrence of reaction (2) (EL-RAGHY and BARSOUM 1998).

Racault et al. (1994) performed the thermal treatment of Ti_3SiC_2 in a graphite crucible under argon atmosphere. The Ti_3SiC_2 used in his studied was manufactured by solid-state synthesis from titanium, silicon and graphite powder in an evacuated silica tube for 10 h at 110 °C. The results show that above 1450 °C Ti_3SiC_2 undergoes to decomposition as presented in reaction (3). However, when samples are in presence of carbon decomposition starts in a temperature range around 1350 °C, favoring formation of SiC (reaction (4)). After such conditions free silicon was found mixed with the graphite crucible and the resulting solid phase from decomposition of Ti_3SiC_2 was $TiC_{0.67}$ (RACAULT, LANGLAIS and NASLAIN 1994).

$$Ti_3SiC_2(s) = 3TiC_{0,67}(s) + Si(g) \quad (3)$$

$$\Delta G\ (1600\ K) = 181\ kJ\ mol^{-1}$$

$$Si(g) + C = SiC \quad (4)$$

$$\Delta G\ (1600\ K) = -\ 276\ kJ\ mol^{-1}$$

Schultheiß, J. (2014) also shows that the decomposition of MAX phase starts above 1350 °C and predicts that the amount of carbon directly influences the temperature and reaction of decomposition of Ti_3SiC_2 into TiC_x (SCHULTHEIß, 2014).

In the present work XRD shows peaks from Ti_8C_5 ($TiC_{0.63}$) and EDS analysis confirms the presence of SiC, what exhibit that both reactions, (3) and (4), occurred. Reaction (3) first happened releasing $Si_{(g)}$ and thereafter causing weight loss as confirmed in section 4.2. When free silicon is in contact with carbon, descendant from dextrin, the reaction 4 occurred forming SiC as showed as spots of SiC phases in SEM analysis.

However, reaction (3) and (4) are dependent, once that reaction (4) will only occur in sites when it has presence of C. On the other hand, reaction (4) is responsible to initiate the decomposition of MAX phase, which corresponds to reaction (3). It's also noted from Figure 22, that the Ti_8C_5 phase, which is formed from Ti_3SiC_2 decomposition is on the

surface of Ti_3SiC_2 grains, evidencing the topotaxial relationship between Ti_8C_5 and Ti_3SiC_2 (RACAULT, LANGLAIS and NASLAIN 1994).

When Si is in presence of carbon the reaction (2) or (3) can happen and thus, avoid escape of $Si_{(g)}$ to atmosphere, that means less weight loss after heat treatment. The weight loss presented in this study exhibits a higher value for samples CIPed with 150 MPa and uniaxially pressed with 726 MPa (6.6 wt% for uniaxially pressed and 6.3 wt% to CIPed samples), what is confirmed by the assumption that full dense samples have a slower reaction kinetic (section 4.4). A higher amount of weight loss for not pressed sample before sintering is also noted. In this event what could have happened is the elimination of carbon during sintering once samples have a higher porosity. In this case, the Si escape due to the less amount of carbon compared with others samples justifying the higher weight loss.

In fact, the thermochemical stability of MAX Phases in general is still not understood and many studies exist about the stability of Ti_3SiC_2 in high temperatures (Oo, Z. *et al.* 2013). For example, Zhang et al. (2008) reported that under nitrogen atmosphere damage and drastic degradation of Ti_3SiC_2 above 1300 °C can occur due to the surface decomposition (Zhang *et al*. 2008). Feng et al. (1999) studied the annealing of Ti_3SiC_2-based bulk samples in vacuum (10^{-2} Pa) and reported that in the samples submitted to 1600 °C for 2 h and 2000 °C for 0,5 h TiCx was found only in the surface (FENG, SATO and WATANABLE, 1999). Barsoum et al. (1996) have shown that Ti_3SiC_2 submitted at 1600 ºC in vacuum for 24 h and in argon atmosphere for 4 h thermodynamically was stable. Beyond that, they also reported that the reduced temperature at which Ti_3SiC_2 decomposed as observed by others was due to the presence of impure phases, like Fe or V, in the feedstock powders, which interfered with the reaction synthesis of Ti_3SiC_2 and thus destabilized following prolonged annealing in an inert environment (TZENOV *et al.* 2000).

4.6. MECHANICAL PROPERTIES

4.6.1. Young's Modulus

The Young's modulus measured at room temperature in an ultrasonic time propagating in horizontal (E_h) and vertical direction (E_v) of Ti_3SiC_2-based structures through the three steps, versus porosity is illustrated in Figure 23.

Figure 23 - Young's Modulus versus porosity for all samples after sintering.

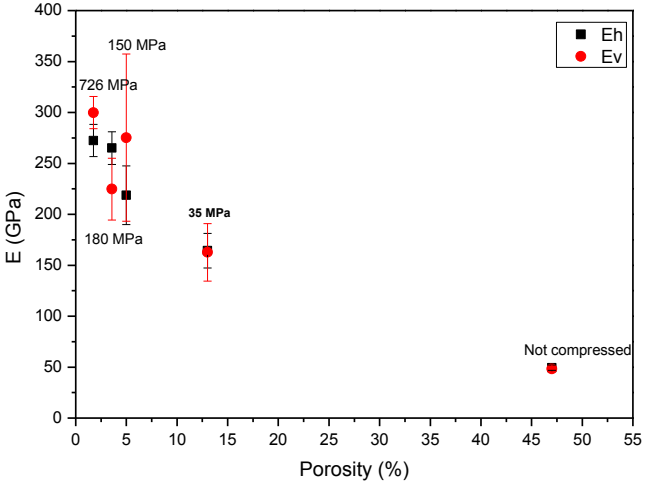

The measurement presented was made by an average of seven test specimens. As expected the Young's modulus increases with the increasing porosity. This can be explained due to the absence of defects in specimens with lower porosity, as pores and cracks (observed in figure 21 and 22).

Table 2 specifies the values of E_h and E_v for each sample after the three steps processing. The highest value of Elastic modulus was found for uniaxially pressed samples at 726 MPa. These values (E_h = 272.5 GPa; E_v = 299.88 GPa) are lower compared to values predicted in literature, equal 320 GPa (320000 MPa) for Young modulus of full dense Ti_3SiC_2 samples (BARSOUM and EL-RAGHY, 1996; ZHOU and SUN, 2000; Sun *et al.*, 2002b).

Table 2- Young's Modulus values for each sample before sintering.

Samples	E_h (GPa)	E_v (GPa)
CIP 180 MPa	265,02	224,78
CIP 150 MPa	218	275
CIP 35 MPa	164,30	162,68
Uniaxial Pressed 726 MPa	272,5	299,88
Not pressed	49,41	48,14

The Young modulus found in this work are a little slower than young modulus predicted in literature. This fact could be attributed to the difference of porosity - once that full dense materials has fewer defects - and due to the different phases though the decomposition of Ti_3SiC_2 (discussed above), which can influence the Young Modulus.

4.6.2. Flexural Strength

Figure 24 shows the values of flexural strength versus porosity of the samples after sintering. The data presented for flexural strength were made from the average of at least five test samples.

Figure 24 - Flexural strength versus porosity for all samples after sintering.

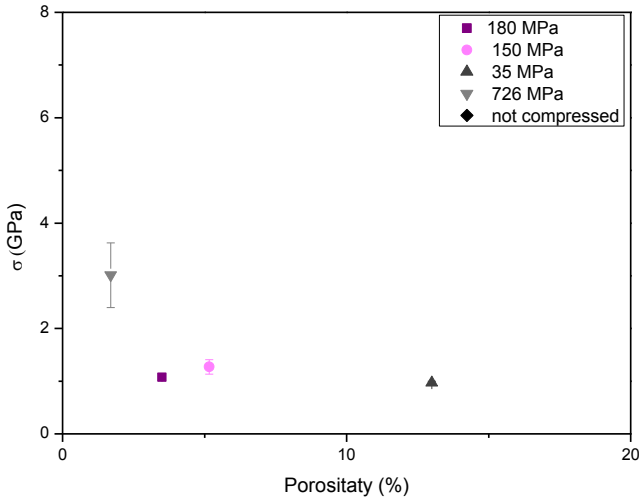

The highest value of flexural strength is for samples uniaxially pressed at 726 MPa before sintering, corresponding to 3,01 GPa. It was expected that the samples with lower porosity obtained higher flexural strength, however only uniaxially pressed samples have a higher flexural strength. The CIPed samples present flexural strength close to the sample not pressed before sintering; perhaps indicating that CIP is not the better path processing to achieve a higher flexural strength compared to uniaxial pressing.

A value of 260 MPa for flexural strength (measured in a four point bending equipment) is predicted in literature for polycrystalline bulk samples of Ti_3SiC_2 synthesized by reactively hot-pressing Ti, graphite and SiC powders at 40 MPa and 1600 °C, for 4 h. This value is one order of magnitude slower, however it is attributed to large grains (~ 100 μm) (EL-RAGHY and BARSOUM, 1996). On the other hand a bulk Ti_3SiC_2 structures via temperature fluctuation synthesis/hot pressing synthesis found a flexural strength equal 470 MPa (ZHOU and SUN, 2000).

5. CONCLUSION AND OUTLOOK

In this work Ti_3SiC_2-based composites were processed via three main steps: three-dimensional printing, uniaxial and cold isostatic pressing and sintering. Beyond that, it showed comparison between two different pressing processing methods and the influence on properties and microstructure of final composites.

The results indicate that uniaxially pressed samples before sintering show a higher density with porosity equal 1.7 wt%. However, SEM analysis showed presence of cracks. CIPed samples before sintering, in turn, presented lower density when compared to uniaxially pressed sample in intermediary stage processing. However, SEM analysis showed a better homogeneity distribution and absence of cracks.

XRD analysis after sintering reports that all specimens exhibit same phases, Ti_3SiC_2 and $TiC_{0,63}$. Samples CIPed at 150 MPa and uniaxially pressed at 726 MPa also presented a carbon peak. The carbon peak in these two kinds of samples is related to the low reactivity between Ti_3SiC_2 and dextrin due to the pressing process. This fact is evidenced by the closer weight loss of both specimens (6.6 wt% for uniaxially pressed and 6.3 wt% to CIPed samples), which indicates Si releasing and not reacting with carbon present in samples.

SEM analysis in disagreement with XRD showed presence of SiC in all samples after sintering. This indicates that Ti_3SiC_2 decomposes in $TiC_{0,63,}$ and $Si_{(g)}$. When $Si_{(g)}$ is in contact with carbon it will react and form SiC. It is important to state that both reactions are dependent. For the decomposition of Ti_3SiC_2 the presence of carbon, which realizes $Si_{(g)}$ is necessary. And the formation of SiC will only happen in the presence of $Si_{(g).}$

Specimens directly sintered after 3D printing showed a higher porosity, which highlights the importance of pressing process before sintering to increase the density. In these samples a poor reactivity between Ti_3SiC_2 and dextrin is also observed. By XRD analysis it is not possible to note peaks of free carbon, suggestion non-evaporation of Si, which is responsible for weight loss and actually burning out of binder (dextrin).

Young's modulus and flexural strength was higher for uniaxially pressed samples before sintering. As expected, Young's modulus decreased with the porosity increasing and flexural strength showed similar values for CIPed and no pressed samples prior sintering, suggesting that CIP does not increase it.

Despite the information that pressing process improves the density, the comparison between CIP and uniaxial pressing in these processing cannot reach full dense ceramics materials and functional ceramic (density above 99%).

Due to the results showed above it is suggested for future researches to investigate the manufacturing of Ti_3SiC_2 by the same route used in this work, however under the same pressure value for both uniaxial and cold isostatic pressing. Once the samples uniaxially pressed under 726 MPa have less porosity compared to samples CIPed with lower pressures. Another prospect is to infiltrate this Ti_3SiC_2-based composite after three-dimensional printing with metals as a different alternative to improve the density and consequently study of new phases and properties of the final composite.

6. REFERENCES

ABU, M. J.; MOHAMED, J. J.; AHMAD, Z. A. Synthesis of high purity titanium silicon carbide from elemental powders using arc melting method. **International Journal of Refractory Metals & Hard Materials,** v. 47, p. 86-92, 2014.

AINSLEY, C.; REIS, N.; B, DERBY. Freeeform fabrication by controlled droplet deposition o powder filled melts. **Journal of Materials Science,** v. 37, p. 3155-3161, 2002.

ARANUJATESAN, S.; CARIM, A. H. Synthesis of Titanium Silicon Carbide. **J. Am. Cerami. Soc,** v. 78, n. 3, p. 667-72, 1995.

BLAZDELL, P. F.; EVANS, J. R. G. Application of continuous ink jet printer to solid freeforming of ceramics. **Journal of Materials Processing Technology,** v. 99, p. 94-102, 2000.

BLAZDELL, P. Solid free-forming of ceramics using a continuous jet printer. **Journal of Materials Processing Technology**, v. 137, p. 49-54, 2003.

CALI, J.; CALIAN, D. A.; AMATI, C.; KLEINBERGER, R.; STEED, A.; KAUTZ, J.; WEYRICH, T. 3D-Printing of Non-Assembly, Articulated Models. **Acm Transactions on Graphics,** v. 31, n. 6, article 130, 2012.

CHEN, I.-W.; WANG, X.-H.Sintering dense nanocrystalline ceramics without final-stage grain growth. Nature, v. 404, n. 9, 2000.

CHUA, C. K.; LEONG, K. F.; LIM, C. S. **Rapid prototyping: principles and applications**. Third edition. Singapore: World Scientific, 2010.

DIMITROV, D.; SCHREVE, K.; DE BEER, N. Advances in three-dimensional printing - state of the art and future perspectives. **Rapid Prototyping Journal,** v.12, n. 3, p. 136-147, 2006.

DIN EN 843-1, Beuth Verlag, GmbH, Berlin (2008)

DIN EN 843-2, Beuth Verlag, GmnH, Berlin (2007)

EL-RAGHY, T.; BARSOUM, M. W. Synthesis and Characterization of a Remarkable Ceramic: Ti_3SiC_2. **J. Am. Ceram. Soc.** V. 79, n. 7, p. 1953-56, 1996.

EL-RAGHY, T.; BARSOUM, M. W. Diffusion kinetics of the carburization and silicidation of Ti_3SiC_2. **Journal of Applied Physics**, v. 83, n. 1, p. 112-119, 1998.

EL-RAGHY, T.; BARSOUM, M. W. Processing and Mechanical Properties of Ti_3SiC_2: I, Reaction Path and Microstructure Evolution. **J. Am. Cerami. Soc,** v. 82, n. 10, p. 2846-54, 1999.

EL-RAGHY, T.; BARSOUM, M. W.; ZAVALIANGOS, A.; KALIDINDI, S. R. Damage mechanisms around hardness indentations in Ti_3SiC_2. **Journal of the American Ceramic Society,** v. 80, n. 2, p. 513-516, 1997.

FENGI, J.; SATO, F.; WATANABLE, R. Synthesis of Ti_3SiC_2 Polycrystals by Hot-Isostatic Pressing of the Elemental Powders. **Journal of Material Science Letters.** V.18, p. 1595-1597, 1999.

FILBERT-DEMUT, I. **Surface Modification of polymer-derived Ceramics**. 2012. (Master thesis)**.** Friedrich-Alexander-Universität Erlangen-Nürnberg, Erlangen-DE, 2012.

FU, Z.; SCHLIER, l.; TRAVITZKY, N.; GREIL, P. Three-dimesioal printing of SiSiC lattice truss structures. **Materials Science & Engineering A**, v. 560, p. 851-856, 2013.

GAO, N. F.; LI, J. T.; ZHANG, D.; MIYAMOTO, Y. Rapid synthesis of dense Ti_3SiC_2 by spark plasma sintering. **Journal of the European Ceramic Society,** v. 22, n. 13, p. 2365-2370, 2002.

GAO, N. F.; MIYAMOTO, Y. Dense Ti_3SiC_2 prepared by reactive HIP. **Journal of Materials Science**, v. 34, p. 4385-4392, 1999.

GILBERT, C. J.; BLOYER, D. R.; BARSOUM, M. W. EL-RAGHY, T. TOMSIA, A. P. RITCHIE, R. O. Fatigue-crack growth and fracture properties of coarse and fine-grained Ti3SiC2. **Scripta Materialia,** v. 42, n. 8, p. 761-767, 2000.

In: <http://www.azom.com/article.aspx?ArticleID=1516>. accessed in: 29/11/2014.

JEE, H. J.; SACHS, E. Avisual simulation technique for 3D printing. **Advances in Engineering Software,** v. 31, p. 97-106, 2000.

JEITSCHKO, W.; NOWOTNY , H. Die Kristallstruktur von Ti3SiC2 - ein neuer Komplexcarbid-Typ. **Mh.Chem**., Bd. 98, 1967.

JIANG, W.; ZHANG, J.; WANG, L.; JIANG, W.; CHEN, L. Effect of TiC content on the Microstructure and Properties of Ti_3SiC_2- Tic composites in situ Fabricated by Spark Plasma Sintering. **Journal of Material Science and Engineering A,** v.487, p. 137-143, 2008.

LEE, William E. **Ceramic microstructures: property control by processing**. London-UK: Springer, 1994.

LIS, J.; MIYAMOTO, Y.; PAMPUCH, R.; TANIHATA, K. Ti_3SiC_2-based materials prepared by HIP-SHS techniques. **Materials Letters**, v. 22, p. 163-168, 1995.

LIS, J.; PAMPUCH, R.; RUDNIK, T.; WEGRZYN, Z. Reaction sintering phenomena of self-propagating high-temperature synthesis-derived ceramic powders in the Ti-Si-C system. **Solid State Ionics,** v. 101, p. 59-64, 1997.

KHALYFA, A.; VOGT, S.; WEISSER, J.; GRIMM, G.; RECHTEBACH, A.; MEYER, W:, SCHABELRAUCH, M. Development of a new calcium phosphate powder-binder system for the 3D printing of patient specific implants. **J. Mater Sci: Mater Med**, v. 18, p. 909-916, 2007.

MELCHER, R.; MARTINS, S.; TRAVITZKY, N.; GREIL, P. Fabrication of Al2O3-based composites by indirect 3D printing. **Materials Letters,** v. 60, n. 4, p. 572-575, 2006.

MELCHER, R.; TRAVITZKY, N.; ZOLLFRANK, C.; GREIL, P. 3D printing of Al2O3/Cu-O interpenetrating phase composite. **Journal of Materials Science,** v. 46, n. 5, p. 1203-1210, 2011.

MORGIEL, J.; LIS, J.; PAMPUCH, R. Microstructure of Ti_3SiC_2-based ceramics. **Materials Letters**, v. 27, p. 85-89, 1996.

MOTT, M.; EVANS, J, R. G. Zirconia/alumina functionally graded material made by ceramic ink jet printing. Materials Science and Engineering, v. A27, p. 344-352, 1999.

NOGUERA, R.; LEJEUNE, M.; CHARTIER, T. 3D fine scale ceramic components formed by ink-jet prototyping process. **Journal of the European Ceramic Society**, v. 25, p. 2055-2059, 2005.

OBERACKER, R. Powder Compaction by Dry Pressing. In: RIEDEL, R. and CHEN, I.-W. **Ceramic Science and Technology: Synthesis and Processing**. Volume 3, third edition. Wiley-VCH Verlag GbmH & Co. KGaA, 2012.

Oo, Z. **Characterization of Thermal Stability, Microstructures and Properties of Al_2TiO_5 - Ti_3SiC_2 based Ceramics.** (PhD Thesis). Curtin University, 2013.

PAMPUCH, R.; LIS, J.; STOBIERSKI, L.; TYMKIEWIEZ, M. Solid Combustion Synthesis of Ti_3SiC_2. **Journal of the European Ceramic Society**, v. 5, p. 283-287, 1989.

PHAM, D. T.; GAULT, R. S. A comparison of rapid prototyping technologies. **International Journal of Machine Tools & Manufacture,** v. 38, n. 10-11, p. 1257-1287, 1998.

RACAUL, C.; LANGLAIS, F.; NASLAIN, R. Solid-State Synthesis and Characterization of the Ternary Phases Ti_3SiC_2. **Journal of Materials Science,** v. 29, p. 3384-3392, 1994.

RADOVIC, M.; Barsoum, M. W. MAX phases: Bridging the gap between metals and ceramics. **American Ceramic Society Bulletin,** v. 92, n. 3, p. 20-27, 2013.

RAMAKRISHNAN, N.; RAJESH, P. K.; PONAMBALAN, P.; PRAKASAN, K. Studies on preparation of ceramic inks and simulation of drop formation and spread in direct ceramic inkjet printing. **Journal of Materials Processing Technology**, v. 169, p. 372-381, 2005.

REED, J. S. Principles of Ceramics Processing. John Wiley & Sons, Inc., New York. 1995.

Riedel, R. Chen, I. Ceramics Science and Technology: Synthesis and processing. Weinheim: WILEY-VCH; 2012. Volume 3.

RILEY, D. P.; KISI, E. H.; HANSEN, T. C.; HEWAT, A. W. Self-propagating high-temperature synthesis of Ti3SiC2: I, ultra-high-speed neutron diffraction study of the reaction mechanism. **Journal of the American Ceramic Society,** v. 85, n. 10, p. 2417-2424, 2002.

RWTH Aachen University. Institute of Mineral Engineering: cold isostatic pressing.

SCHLIER, L; ZHANG, W.; TRAVITZKY, N.; GREIL, P.; CYPRIS, J.; WEDAS, M. Macro-Cellular Silicon carbide Reactors for Nonstationary Combustion Under Piston Engine-Like Conditions. **Applied Ceramics Technology.** v. 8, n. 5, p. 1237-1245, 2011.

SCHULTHEIß, J**. Processing and Characterization of Paper-derived MAX phase ceramics.** 2014**.** (Master thesis). Friedrich-Alexander-Universität Erlangen-Nürnberg, Erlangen-DE, 2014.

SERDEEN, K. A. M.; REIS, N.; EVANS, J. R. G.; PATRICK, S. G.; HALLORAN, J. W.; DERBY, B. Ink-Jet Printing of Wax-Based Alumina Suspensions. **J. Am. Ceram. Soc.**, v. 84, n. 11, p. 2514-20, 2001.

SHUI, A.; KATO, Z.; TANAKA, S.; UCHIDA, N.; UEMATSU, K. Sintering deformation caused by particle orientation in uniaxially and isostatically pressed alumina compacts. **Journal of the European Ceramic Society**, v. 22, p. 311-316, 2002.

SINGH, R. Three Dimensional Printing for Casting Applications: A State of Art Review and Future Perspectives. **Advances in Materials and Processing Technologies, Pts 1 and 2,** v. 83-86, p. 342-349, 2010.

SLADE, C. E.; J. R. G. EVANS. Freeforming ceramics using a thermal jet printer. **Journal of Materials Science Letters**, v. 17, p.1669-1671, 1998.

SONG, J. H.; EDIRISIGHE, M. J.; EVANS, J. R. G. Formulation and Multilayer jet printing of ceramic Inks. J. **Am. Ceram. Soc.**, v. 82, n. 12, p. 3374-80, 1999.

SUN, W.; DCOSTA, D. J.; LIN, F.; EL-RAGHY. T. Freeform Fabrication of Ti_3SiC_2. Powder based Structures Part I: Integrated Fabrication Process. **Journal of Materials Processing Technology**, v. 127, p. 343-351, 2002a.

SUN, W.; DCOSTA, D. J.; LIN, F.; EL-RAGHY. T. Freeform Fabrication of Ti_3SiC_2. Powder based Structures Part II: Characterization and Microstructure Evolution. **Journal of Materials Processing Technology**, v. 127, p. 352-360, 2002b.

SUN, Z. M. Progress in research and development on MAX phases: a family of layered ternary compounds. **International Materials Reviews,** v. 56, n. 3, p. 143-166, 2011.

TAY, B. Y.; EVANS, J. R. G.; EDIRISINGHE, M. J. Solid freeform fabrication of ceramics. **International Materials Reviews,** v. 48, n. 6, p. 341-370, 2003.

TONG, X. H.; OKANO, T.; ISEKI, T.; YANO, T. Synthesis and High-Temperature Mechanical-Properties of Ti3sic2/Sic Composite. **Journal of Materials Science,** v. 30, n. 12, p. 3087-3090, 1995.

TRAVITZKY, N.; BONET, A.; DERMEIK, B.; FEY, T.; FILBERT-DEMUT, I. SCHLIER, L.; SCHLORDT, T.; GREIL, P. Additive Manufacturing of Ceramic-Based Materials. **Advanced Engineering Materials,** v. 16, n. 6, p. 729-754, 2014.

TSENG, W. J.; LIN, S.-Y.; WANG, S.-R. Particulate dispersion and freeform fabrication of $BaTiO_3$ thick films via direct inkjet printing. **J. Electroceram**., v. 16, p. 537-540, 2006.

TURNER, C. D.; ASHBY, M. F. The cold isostatic pressing of composite powder – I. experimental investigations using model powders. **PII**. V. 00064-x, p. 4521-4530, 1996

TZENOV, N.; BARSOUM, M. W.; EL-RAGHY, T. Influence of Small Amounts of Fe and V on the Synthesis and Stability of Ti_3SiC_2. **Journal of European Society.** V.20, p. 801-801, 2000.

VEIGA, M. D.; MERINO, M.; FERNADEZ, D.; LOZANO, R. Characterization of Some Cyclodextrin Derivates by Thermal Analysis. **Journal of Thermal Analysis and Calorimetry,** v.68, p.511-516, 2002.

WAKELKAMP, W. J. J.; VAN LOO, F. J. J.; METSELAAR, R. Phase Relations in the Ti-Si-C System. **Journal of the European Ceramic Society**, v. 22, p. 2365-2370 2002.

ZHANG, H.; YANCHUN, Z.; YIWANG, B.; MEISHUAN, L. Titanium Silicon Carbide Pest Induced by Nitridation. J**. Am. Ceram. Soc**, v. 91, n. 2, p. 494-499, 2008.

ZHAO, X.; EVANS, J. R. G.; EDIRISINGHE, M. J.; Song, J. H.; Formulation of Ceramic ink for a wide-array drop-on-demand ink-jet printer. **Ceramic International,** v. 29, p. 887-892, 2003.

ZHOU, Y. C.; SUN, Z. M. Electronic structure and bonding properties in layered ternary carbide Ti3SiC2. **Journal of Physics-Condensed Matter,** v. 12, n. 28, L457-L462, 2002.

ZHOU, Y.; SUN, Z. Temperature fluctation/hot pressing synthesis of Ti_3SiC_2. **Journal of Materials Science,** v. 35, p. 4343-4346, 2000.